Taylor & Francis
Taylor & Francis Group

Check for updates

Precipitation as a key control on erosion rates in the tectonically inactive northeastern Sonoran Desert, central Arizona, USA

Ara Jeong [a], Yeong Bae Seong [b], Ronald I. Dorn [c] and Byung Yong Yu [d]

aDepartment of Civil Engineering and Environmental Sciences, Korea Military Academy, Seoul, Republic of Korea; bDepartment of Geography Education, Korea University, Seoul, Republic of Korea; cSchool of Geographical Sciences and Urban Planning, Arizona State University, Tempe, USA; dLaboratory of Accelerator Mass Spectrometry, Korea Institute of Science and Technology, Seoul, Republic of Korea

ABSTRACT

Langbein and Schumm (1958) connected precipitation to erosion in a right-skewed curve used in earth science textbooks for over six decades, where denudation increases with precipitation on the arid/semiarid limb and decreases in humid regions. Development of the catchment-averaged ^{10}Be denudation method a quarter-century ago led geomorphologists to evaluate this hypothesis using data not influenced by the Anthropocene, with mixed findings. The Sonoran Desert in Arizona, USA, is optimal for investigating the longstanding hypothesis of increased erosion from arid to semiarid climates due to: (i) the modern orographic effect aligning elevated precipitation with altitude, mirroring *Neotoma* packrat midden paleoecology research for the Holocene and late Pleistocene; (ii) the region has been tectonically quiet for the residence times of analyzed ^{10}Be ranging from ca. 8,000-110,000 years. Our significant finding echoes Langbein and Schumm's work, revealing heightened erosion along an elevation-precipitation gradient from arid to semiarid conditions. Notably, the significance of precipitation-elevation contrasts with the absence of significant correlation between ^{10}Be denudation and attributes like slope, drainage area, relief, or landform type (e.g., alluvial fan, pediment, mountain watershed). Modern faunalturbation, increasing along this gradient, exposes more ground to rainsplash and overland flow at higher elevations, adding complexity to these results. Further insights unveil that (i) catchments in areas with substantial Quaternary base level reduction imitate tectonic effects, tripling ^{10}Be denudation rates; (ii) basaltic boulders and cobbles yield an armoring influence; (iii) historical erosion acceleration due to urbanization and wildfires insignificantly affects ^{10}Be denudation rates in the Sonoran Desert; and (iv) minute desert catchments yield anomalous erosion rates.

CONTACT Ara Jeong ✉ ara.jeong.research@gmail.com; ara_jeong@kma.ac.kr 🖂 Department of Civil Engineering and Environmental Sciences, Korea Military Academy, Seoul, Republic of Korea

Supplemental data for this article can be accessed online at https://doi.org/10.1080/02723646.2023.2251654.

Introduction

Cosmogenic nuclides in detrital sediments have seen widespread use in estimating catchment-averaged denudation rate over timescales of 10^3-10^5 years since the mid-1990s (e.g. Granger & Schaller, 2014; Granger et al., 1996; Kim et al., 2016; Lee et al., 2021; Placzek et al., 2014; von Blanckenburg, 2005). The catchment-averaged ^{10}Be denudation rate technique assumes that soil or regolith erodes at a steady state (Granger & Schaller, 2014). Sudden exposures of sediment at depth, which can occur in landslides, would invalidate the method if they were widespread in the catchment. Where steady state soil erosion exists, the concentration of cosmogenic nuclides in stream sediments reflects a spatially average denudation rate for an entire watershed, if (i) the time of sediment storage and transport << the time taken to erode by 60 cm of bedrock ("effective exposure time"), and (ii) an even spatial distribution of quartz occurs over the watershed (Reiners et al., 2017).

The typical timescales measured by catchment-averaged ^{10}Be denudation rates range from early Holocene to ca. 100 ka, and hence the measured denudation reflects a number of processes such as rock decay (weathering), soil formation, glacial-interglacial climate change, river incision/aggradation and also potentially the Anthropocene (Granger & Schaller, 2014). Since catchment-averaged ^{10}Be denudation rates represent long-term average denudation rate, an abundance of high-magnitude and low-frequency events over a period of time can sometimes be captured.

The catchment-averaged ^{10}Be denudation rate technique, however, appears to be relatively insensitive to modern sediment erosion over decadal or centennial timescales, as measured by stream gages (Covault et al., 2013; Kirchner et al., 2001). Catchment-averaged ^{10}Be denudation rate measurements in landscapes disturbed by human activities (Hawkins, 2003; Reusser et al., 2015), gullying and piping (Gellis et al., 2004) do not match modern erosion measurements, indicating that the method does not record historic high-magnitude and low-frequency erosion events.

Several studies of compiled catchment-averaged ^{10}Be denudation rates across the globe sought to find controlling factors on denudation (Harel et al., 2016; Mishra et al., 2019; Portenga & Bierman, 2011; von Blanckenburg, 2005; Willenbring et al., 2013). Slope appears to be an important control on catchment-averaged ^{10}Be denudation rates (Portenga & Bierman, 2011; Willenbring et al., 2013), while some found that climate-related variables (precipitation and temperature) showed no meaningful relationship with catchment-averaged ^{10}Be denudation rate (Harel et al., 2016; Portenga & Bierman, 2011; von Blanckenburg, 2005; Willenbring et al., 2013), leading to a conclusion that tectonics, rather than climate, controls millennial-scale erosion (Granger & Schaller, 2014).

In contrast, a recent study found mean annual precipitation (MAP) to be important in regulating denudation rates (Mishra et al., 2019). In particular, Mishra et al. (2019) consider MAP to be important in arid (MAP: 0–1050 mm yr^{-1}) and hyper-wet areas (MAP: >2200 mm yr^{-1}). However, vegetation cover dampens the role of precipitation in watersheds with MAP between 1050 and 2200 mm yr^{-1} (Mishra et al., 2019).

Prior catchment-averaged ^{10}Be denudation rate research also evaluated the role of rock type but failed to find a significant correlation in synthesizing global data (Portenga & Bierman, 2011). Local to regional scale ^{10}Be denudation studies also suggested that

lithology plays a less important role on denudation (Dirks et al., 2016; Duxbury et al., 2015). Exceptions, however, exist; for example, granite grussification leads to statistically separable and faster catchment-averaged ^{10}Be denudation rates than quartzite catchments (Duxbury et al., 2015; Kim et al., 2022).

Our approach in this paper explores the long-asked (e.g. Langbein & Schumm, 1958) research question of whether precipitation influences millennial-scale erosion along an arid to semi-arid gradient. Different from prior research, we focus solely on catchment-averaged ^{10}Be denudation rates in a (i) tectonically inactive landscape that (ii) exhibits a modern-day and late-Quaternary precipitation gradient from arid and semi-arid. Both conditions are met in the Sonoran Desert in central Arizona, USA, allowing us to separate tectonic and climate controls on erosion.

Some cosmogenic ^{10}Be research suggests that climate may, however, also connect sediment transport to bioturbation (Wackett et al., 2018). In our study region of the Sonoran Desert, small animals burrow underneath and around the margins of perennial shrubs in the upper 20 cm of soils, creating surface mounds of dug-up sediment (Hembree et al., 2017; Lee, 1986). Faunalturbation (Butler, 1995; Cavin & Butler, 2015), thus, exposes fines to rainsplash and overland flow. Erosion rates from animal burrowing in Chile increase from 0.34 m^3 ha^{-1} yr^{-1} in an arid setting to 0.56 m^3 ha^{-1} yr^{-1} in a semi-arid climate (Übernickel et al., 2021). Thus, in evaluation of the role of precipitation on catchment-averaged ^{10}Be denudation rates, it is possible that faunalturbation could be an important factor in long-term erosion rates along an arid to semi-arid transition. Certainly, modern measurements of mounds from animal burrows can only be related to modern erosion rate measurements. At the same time, climate change could shift faunalturbation impacts spatially (Coggan et al., 2018). Thus, in order to better understand the connection between precipitation, erosion, and faunalturbation, we also undertook an investigation to understand how mound density from animal burrowing changes with elevation in studied catchments.

Jeong and Dorn (2019) found that human activities associated with urban expansion significantly increased modern sediment yield. Hence, to understand the role of climate, this research must also rule out the role of human activities on catchment-averaged ^{10}Be denudation rates in this arid urban setting. After determining that the Anthropocene does not influence the catchment-averaged ^{10}Be denudation rate method in an urbanizing desert setting, we could then focus on finding controlling variables of ^{10}Be catchment-averaged ^{10}Be denudation rats testing here the hypothesis that precipitation is an important driver of millennial-scale erosion along an arid to semi-arid gradient with quiescent tectonism.

Research setting

Regional setting

Arizona, USA, has a complex geological history (Eaton, 1982; Spencer & Reynolds, 1989; Spencer et al., 2001) with the southern part of the state being dominated by the Basin and Range Province (BRP) and extensional tectonics, the northeastern corner occupied by flat-lying sedimentary rocks of the Colorado Plateau and a transition zone between them. The climatological Sonoran Desert rests mostly within the BRP at elevations mostly
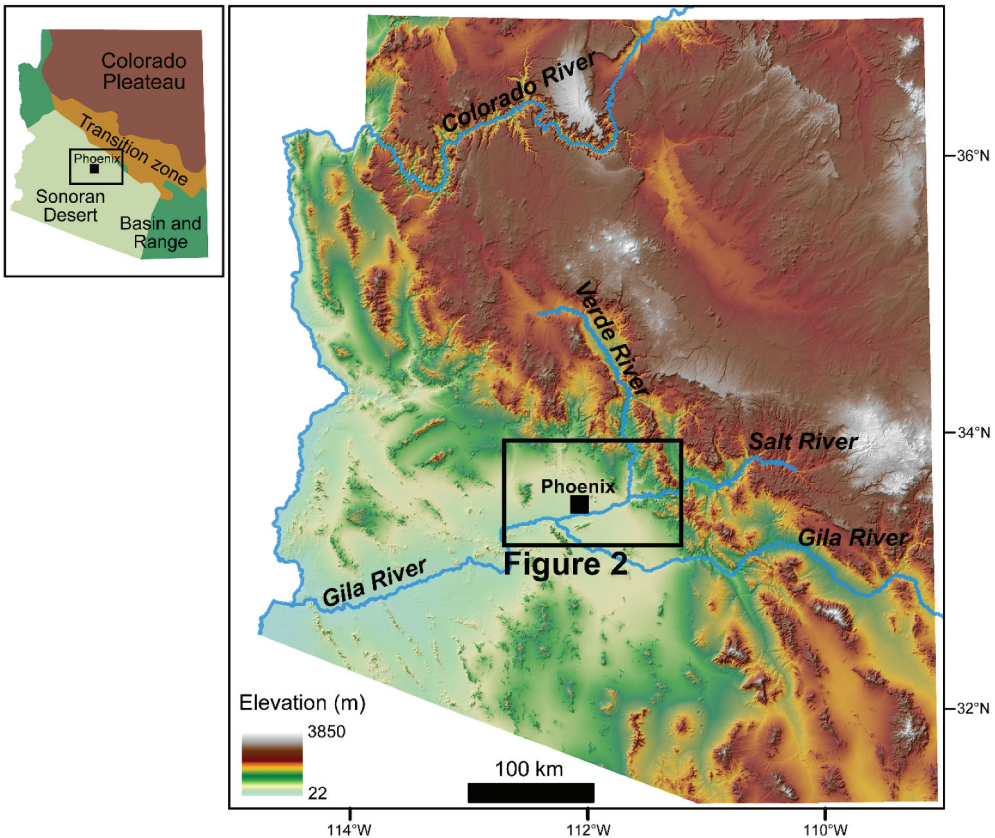
Figure 1. Topographic map of the Arizona, USA with studied watersheds found within the box. This study area occurs in the climatological Sonoran Desert and within geological basin and range province where the Salt, Verde and Gila rivers flow through the Phoenix metropolitan region.

below 1200 m. Our study area varies in elevation from ca. 450 to 900 m in the central part of Arizona (Figure 1) – all in the northeast corner of the Sonoran Desert.

The BRP in Arizona started to extend in the Oligocene (Chapman et al., 2019; Eaton, 1982; Spencer et al., 2001). High heat flow and strain rates generated extension along normal faults in the early Miocene (Spencer & Reynolds, 1991). Crustal cooling then took place in the middle and late Miocene, with high-angle normal faulting leading to grabens and half-grabens. Active faulting slowed in late Miocene, and down-faulted basins filled with sediment. Local Plio-Pleistocene subsidence led to the location of depocenters in endorheic basins (Skotnicki & DePonty, 2020). At least three young faults with presumed or demonstrable late Quaternary offset are exposed north and east of the study area (Leighty et al., 1997; Pearthree & Scarborough, 1985; Skotnicki, 1996; Skotnicki & Leighty, 1997). However, the flat-lying playa deposits in the structural basins in the study area indicate that faulting waned probably near the beginning of the Pliocene (Skotnicki & DePonty, 2020). Gootee (2013) also found minimal evidence of tectonic activity in the Pliocene or Quaternary in the study area.

Exposed bedrock (Figure 2) represents a complex mix of rock types and ages in the study area (Richard et al., 2002). Neogene volcanics outcrop as basalts and felsic eruptions from calderas (Shafiqullah et al., 1980). These extrusive rocks, as
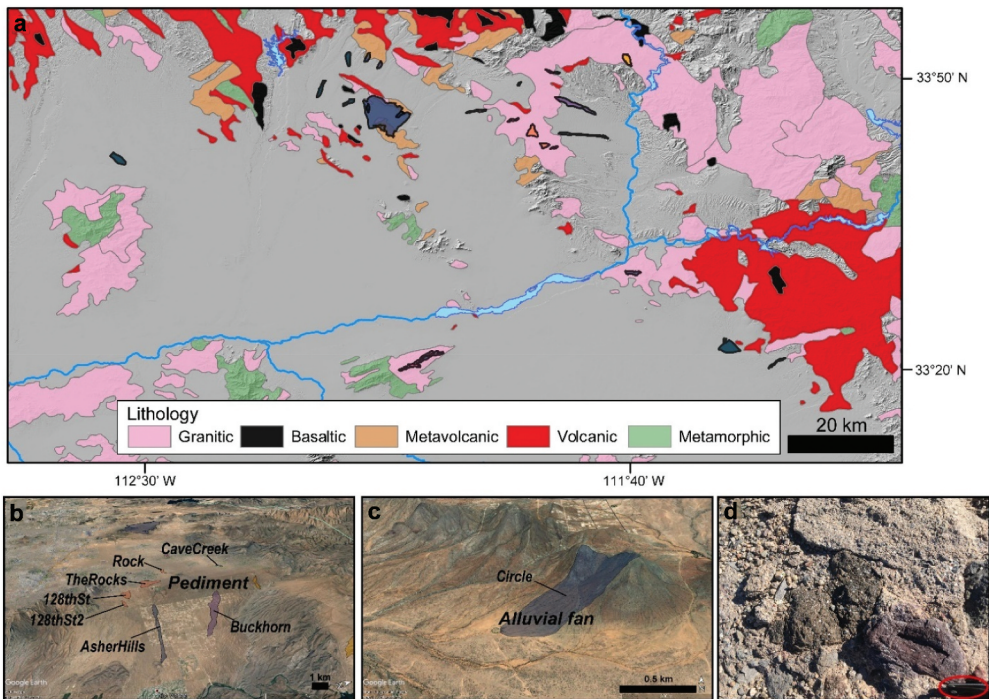
Figure 2. Geologic and geomorphic setting of studied catchments. (a) geologic map of the study region overlaid by studied catchments. Granitic rocks range from granodiorite to diorite. The label "volcanic indicates rocks with a felsic composition, often derived from caldera eruptions. Metamorphic rocks include metavolcanic, metasedimentary, and gneissic compositions. (b) example of catchments developed on pediments, where names match data tables. (c) example of a catchment developed on alluvial fan. (d) field observation of sediments in the Cline catchment – where no basalt flows were mapped, but there are still big boulders and cobbles with basaltic and andesitic (reddish material) composition with scale provided by the circled sunglasses. Metamorphic and granitic materials supply gravel and sand-sized materials. Elevations in Google Earth satellite images are vertically 3× exaggerated.

well as metamorphic lithologies, generate a wide range of sediment sizes in ephemeral washes ranging from boulders to clay. Granitic rock types, in contrast, decays to grus, generating much of the sand observed in the drainage networks of the region.

During the Pliocene, endorheic basins started to overspill sediment into lower basins, but sediment transport was by ephemeral flow only (Skotnicki et al., 2021). Also, in the Pliocene, the Salt, Verde, and Gila rivers of Arizona (Figure 1) integrated into exoreic rivers through a combination of lake overflow and subsequent knickpoint retreat into the former lake basin (Skotnicki et al., 2021). Prior to river integration, closed-basin piedmonts consisted of a mixture of pediments and alluvial fans (Figure 2b & 2c). The geomorphology of these desert piedmonts responded in complex ways to river integration, but the net result produced incision of both pediments and alluvial fans throughout the study area (González et al., 2022).

Sampled catchments

The sampled catchments (Table 1) vary in size from 0.2 km² to 33.4 km², and range in relief from 15 m to 360 m. A supplemental Google Earth KML file allows readers the ability to examine sampled catchments in detail. These study sites were originally selected for different purposes. Most of them are associated with a study of the impact of land-use changes on historic sediment yields (Jeong & Dorn, 2019; Jeong et al., 2021). Others were part of an evaluation of the process-domain model of Montgomery (1999) in an arid setting (Seong et al., 2016). Two more were originally sampled to study the impact of wildfire on erosion rates. Data from catchments evaluated to study historic erosion (Jeong et al., 2021), and nine catchments presented by Seong et al. (2016) are repurposed for this study testing the importance of precipitation on erosion in the Sonoran Desert. We present here for the first time ^{10}Be denudation data for seven additional catchments.

These small watersheds represent all known ^{10}Be catchment averaged denudation rates in the study area (Figure 3). Their distribution and elevations align with a southwesterly frontal storm flow. Rainfall increases from the southwest to the northeast direction as elevations rise due to an orographic effect (Bruintjes et al., 1994; Hawkins, 2003; Hughes et al., 2014; Karnieli, 1990; Shinker & Bartlein, 2010).

The sampled catchments are found in three basic geomorphic settings (Figure 3). Those sampled to evaluate the process-domain model occur entirely within the bedrock granitic range of the eastern half of South Mountains (Seong et al., 2016). Four catchments occur within metavolcanic-dominated mountainous watersheds. The remaining catchments are evenly divided between alluvial-fan surfaces and pediments.

Materials and methods

Data used to evaluate possible controls on ^{10}Be denudation rates

In order to understand and evaluate possible influences on ^{10}Be erosion rates, we collected quantitative and qualitative data for each of catchments. ArcGIS software generated morphometric parameters such as drainage area, average slope, and maximum relief using a USGS 3DEP 1/3 arc-second (~10 m) resolution DEM (U.S. Geological Survey, 2017; available at https://viewer.nationalmap.gov/basic/).

Compiled climatic parameters are based on 30-year averages of annual precipitation totals, seasonal precipitation totals, number of days during the year with precipitation ≥ 1 inch, and annual average temperature from 22 meteorological stations of NOAA U.S. annual/seasonal climate normals (1981–2010) (Arguez et al., 2010; available at https://gis.ncdc.noaa.gov/maps/ncei/normals) (Table S1).

We compiled rock types using geological maps (Richard et al., 2002) as well as direct field observations. We generalized landform setting into three categories: catchment exists entirely within a range; catchment on an alluvial fan; and catchment on a pediment.

Relationship between ^{10}Be denudation rate, elevation, precipitation, and rock type in central Arizona

After we determined that the PIMA055/055a and PIMA056/056a samples were not significantly different, we averaged these values because the samples were collected

Table 1. Catchment information, including location, slope, area, relief, rock type, landform and ^{10}Be denudation rate.

Dataset S1 - Sample basin location data

Sample ID	Latitude (°)	Longitude (°)	Mean elev. (m asl)	Avg. basin slope (°)	Basin area (km²)	Basin relief (m)	Landform	Rock type	^{10}Be erosion rate ± 1σ (m My⁻¹)[a]	Timescale ± 1σ (ky)[b]	Recent disturbance?	Reference
1. Cigar	33.68500	-112.53436	462	0.4	2.6	18	Alluvial fan	metamorphic, basalt, granite	5.3±0.3	111.6±1.2		Jeong et al. (2021)
2. Saguaro	33.80142	-112.20419	496	0.7	1.4	33	Alluvial fan	metamorphic, basalt, granite	8.8±0.6	67.3±0.8		Jeong et al. (2021)
3. Cline	33.85575	-112.14922	569	1.2	1.5	42	Holocene fan	metamorphic, basalt, granite	5.2±0.3	113.3±1.4		Jeong et al. (2021)
4. Anthem	33.85057	-112.10162	612	6.2	0.9	209	Foothills drainage basin	metavolcanic	14.0±0.9	42.3±0.6		Jeong et al. (2021)
5. Anthem2	33.85172	-112.09986	586	1.8	0.6	40	Foothills drainage basin	metavolcanic	19.2±1.2	30.9±0.5		Jeong et al. (2021)
6. Pepe	33.78610	-112.15994	496	0.6	1.0	21	abandoned fan	metamorphic, basalt, granite	6.2±0.4	95.1±1.1		Jeong et al. (2021)
7. Bronco	33.77539	-112.11689	497	0.6	0.5	15	Holocene fan	metamorphic, basalt, granite	7.9±0.5	75.5±0.9		Jeong et al. (2021)
8. Circle	33.77117	-112.06117	538	6.5	0.6	153	Alluvial fan	metamorphic	13.3±0.9	44.6±1.1		Jeong et al. (2021)
9. Charlie	33.77425	-111.94944	675	1.2	0.9	72	alluvial slope	granitic	21.2±1.3	28.0±0.5		Jeong et al. (2021)
10. Rock	33.75981	-111.87647	772	2.6	0.5	59	Pediment	granitic	32.5±2.6	18.2±1.0		Jeong et al. (2021)
11. CaveCreek	33.82148	-111.86004	865	1.9	0.2	25	Pediment (dissecting)	granitic	7.2±0.5	82.3±0.9		Jeong et al. (2021)
12. Buckhorn	33.77156	-111.72667	743	1.5	4.4	203	Pediment (dissecting)	granitic	15.4±1.0	38.5±0.6		Jeong et al. (2021)
13. TheRocks	33.73597	-111.84075	825	2.2	2.4	68	Pediment	granitic	31.7±2.0	18.7±0.4		Jeong et al. (2021)
14. 128thSt	33.71972	-111.80633	817	1.7	0.9	32	Pediment (dissecting)	granitic	34.6±2.2	17.1±0.4		Jeong et al. (2021)
15. 128thSt2	33.71642	-111.79117	783	1.7	0.3	37	Pediment (dissecting)	granitic	31.4±2.0	18.9±0.5		Jeong et al. (2021)
16. AsherHills	33.73025	-111.70503	671	1.3	2.1	196	Pediment (dissecting)	granitic	14.5±0.9	40.9±0.6		Jeong et al. (2021)

(Continued)

Table 1. (Continued).

Dataset S1 - Sample basin location data

Sample ID	Latitude (°)	Longitude (°)	Mean elev. (m asl)	Avg. basin slope (°)	Basin area (km²)	Basin relief (m)	Landform	Rock type	^{10}Be erosion rate ± 1σ (m My^{-1})[a]	Timescale ± 1σ (ky)[b]	Recent disturbance?	Reference
17. GoldCyn	33.36767	-111.51497	514	0.6	5.1	33	alluvial slope	ignimbrite, granitic	10.0±0.6	59.3±0.9		Jeong et al. (2021)
18. Peralta	33.33498	-111.42951	577	2.0	0.8	49	Pediment (dissected)	ignimbrite, granitic, breccia	27.1±1.7	21.9±0.5		Jeong et al. (2021)
19. CAPC01	33.74938	-112.11364	517	4.9	33.4	239	Alluvial fan	granitic, metavolcanic	11.1±0.7	53.4±0.6		Jeong et al. (2021)
20. CAPC02	33.75120	-112.09844	557	18.3	0.8	189	Mountain	metavolcanic	14.9±0.9	39.8±0.5	No Construction	Jeong et al. (2021)
21. CAPC03	33.75258	-112.10775	542	15.3	0.9	210	Mountain +pediment	metavolcanic	13.6±0.8	43.6±0.6	Construction	Jeong et al. (2021)
22. CCCf01	33.85503	-111.66509	893	12.5	1.8	272	Mountain slope	granitic	76.9±4.9	7.7±0.2	Burn	This study
23. CCCf02	33.84239	-111.78841	873	6.1	0.6	144	Mountain slope	granitic	68.9±5.0	8.6±0.4	No burn	This study
24. PIMA051	33.36227	-111.99012	578	15.4	3.3	360	Mountain	granitic	20.9±3.3	28.4±4.1		Seong et al. (2016)
25. PIMA052	33.36274	-111.99622	593	15.5	3.0	339	Mountain	granitic	18.9±1.9	31.4±2.5		Seong et al. (2016)
26. PIMA053	33.36124	-112.00418	611	15.2	2.5	310	Mountain	granitic	21.6±1.9	27.4±1.8		Seong et al. (2016)
27. PIMA055	33.35996	-112.00562	639	15.7	1.6	297	Mountain	granitic	18.7±5.6	31.7±9.1	Pre-storm	Seong et al. (2016)
28. PIMA055a	33.35996	-112.00562	639	15.7	1.6	297	Mountain	granitic	18.1±5.2	32.7±9.0	Post-storm	Seong et al. (2016)
29. PIMA056	33.35574	-112.01492	663	14.2	1.2	206	Mountain	granitic	14.2±4.4	41.7±12.4	Pre-storm	Seong et al. (2016)
30. PIMA056a	33.35574	-112.01492	663	14.2	1.2	206	Mountain	granitic	14.5±1.2	40.9±2.3	Post-storm	Seong et al. (2016)
31. PIMA057	33.35090	-112.02203	691	13.4	0.7	151	Mountain	granitic	17.6±5.3	33.7±9.7		Seong et al. (2016)
32. PIMA058	33.34760	-112.02897	708	13.2	0.4	107	Mountain	granitic	20.9±5.5	28.4±7.1		Seong et al. (2016)

(Continued)

Table 1. (Continued).

Dataset S1 - Sample basin location data

Sample ID	Latitude (°)	Longitude (°)	Mean elev. (m asl)	Avg. basin slope (°)	Basin area (km²)	Basin relief (m)	Landform	Rock type	10Be erosion rate ± 1σ (m My⁻¹)[a]	Timescale ± 1σ (ky)[b]	Recent disturbance?	Reference
33. CDL059	33.33596	-112.05373	763	13.0	0.3	98	Mountain	granitic	16.5±2.4	35.9±4.5		This study
34. CDL060	33.34023	-112.04582	741	13.4	0.7	145	Mountain	granitic	24.5±2.3	24.2±1.7		This study
35. CDL061	33.33870	-112.03144	705	19.8	1.5	301	Mountain	granitic	25.1±2.3	23.6±1.6		This study
36. CDL062	33.33707	-112.02828	695	20.6	1.6	351	Mountain	granitic	18.0±1.5	32.9±1.9		This study
37. HAWES	33.50232	-111.67500	568	11.8	1.3	270	Usery Mount-Pediment	granitic	14.3±0.9	41.4±0.5		This study

[a]CRONUS erosion rate calculator version 3 (Balco et al., 2008) with time-dependent LSDn scaling scheme (Lifton et al., 2014) was used to calculate erosion rates.
[b]Timescale indicates the duration over which one penetration length of the surface in the basin ($Λ/ρ= \sim 60$ cm) erodes.
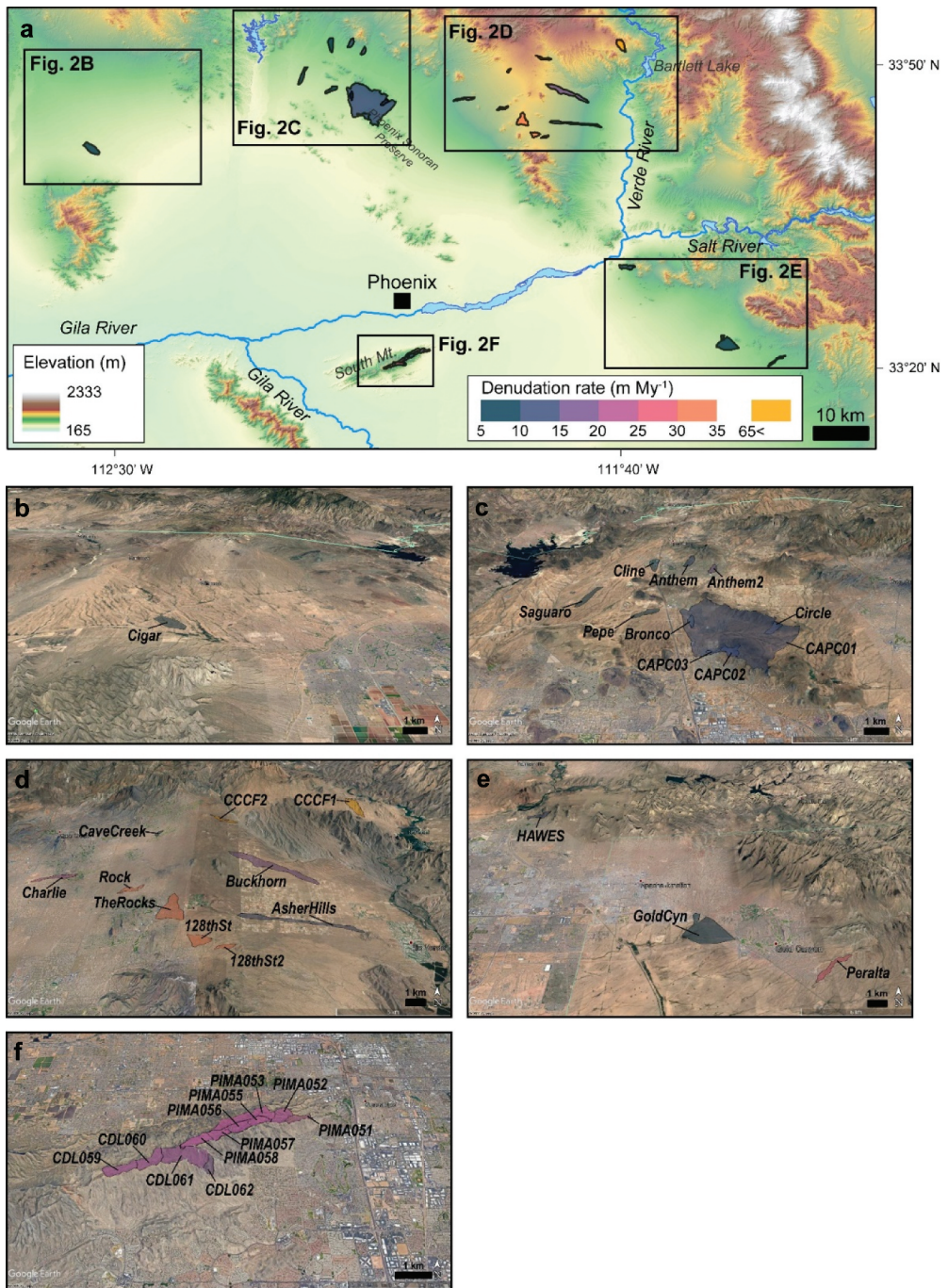
Figure 3. Studied catchments. (a) map of study sites with new and previously published [10]Be catchment-averaged denudation rates from 37 catchments. (b) Northwest sector of study area, showing the Cigar catchment on alluvial fan. (c) Northern sector of the study area dominated by metavolcanic rocks with some basalt. (d) northeast sector of the study area dominated by granitic pediments. (e) southeastern pediment and alluvial slope catchments dominated by ignimbrite and granitic rocks. (f) southeastern granitic catchments within the granitic Guadalupe range of South

from exactly the same catchments, before and after a large rain event. To examine the relationship between ^{10}Be denudation rate and catchment geomorphological factors (i.e. mean elevation, mean slope, drainage area, relief), we completed a statistical analysis correlation matrix, as well as simple linear regression (table S2 and Figure S1). Independent-sample t-tests compared catchment-averaged ^{10}Be denudation rates in study areas with previously published rates and also compared rates in different rock types (Table S3).

Methods to estimate ^{10}Be-derived catchment denudation rates

Detrital ^{10}Be provides an opportunity to calculate temporally and spatially averaged catchment-wide erosion rate using fluvial sediments at the mouth of a watershed (Granger et al., 1996), because surficial sediments are transported to downstream and homogenized (von Blanckenburg, 2005). We collected new samples from seven small basins, and we repurposed in a completely new way results from samples collected previously from 37 active channels of small basins in the previous field campaigns (2014, 2016, 2017 and 2019) in the study area (Figure 1). Fluvial sediments were sieved by collecting the 250–750 μm grain size fraction on site.

This 250–750 μm size fraction was then chemically treated (Kohl and Nishiizumi, 1992) at the Geochronology Laboratory at Korea University, Seoul, Korea. The treatment repeatedly etches minerals in a dilute HF/HNO$_3$ mixture (Kohl and Nishiizumi, 1992). We added a ^{9}Be carrier with a ^{10}Be/^{9}Be ratio $<3.0 \times 10^{-15}$, then separated and purified the Be by ion-exchange chromatography and selective precipitation of BeOH at pH >7. BeOH was oxidized by ignition in a quartz crucible at 800℃ for 10 min (Jeong et al., 2018). BeO was then mixed with Nb metal and loaded onto targets for the measurement of the ^{10}Be/^{9}Be ratio by the 6 MV accelerator mass spectrometry (AMS) at the facility of Korea Institute of Science and Technology (KIST), Seoul, Korea (Jeong et al., 2018). Isotope ratios were normalized to the ^{10}Be standards (Nishiizumi et al., 2007) and the measured isotope ratios were converted to cosmogenic ^{10}Be concentrations in quartz using the total ^{10}Be in the samples and sample weights. We calculated ^{10}Be-derived catchment averaged erosion rates using the online calculators on http://hess.ess.washing ton.edu/(version 3) (Balco et al., 2008) with the time-dependent LSDn scaling scheme (Lifton et al., 2014).

Evaluating the impact of historic events on Sonoran desert denudation

Calculating catchment-averaged ^{10}Be denudation rates assumes that short-term historic events will not influence spatially averaged rates of denudation that measure timescales of thousands to hundreds of thousands of years (Granger et al., 1996). However, given the relatively limited research conducted on

Mountains. ^{10}Be catchment-averaged denudation rates of PIMA051-PIMA058 were previously published (Seong et al., 2016). CDL059-CDL062 are newly presented in this paper. (b-f) elevations in Google Earth satellite images are vertically 3× exaggerated.
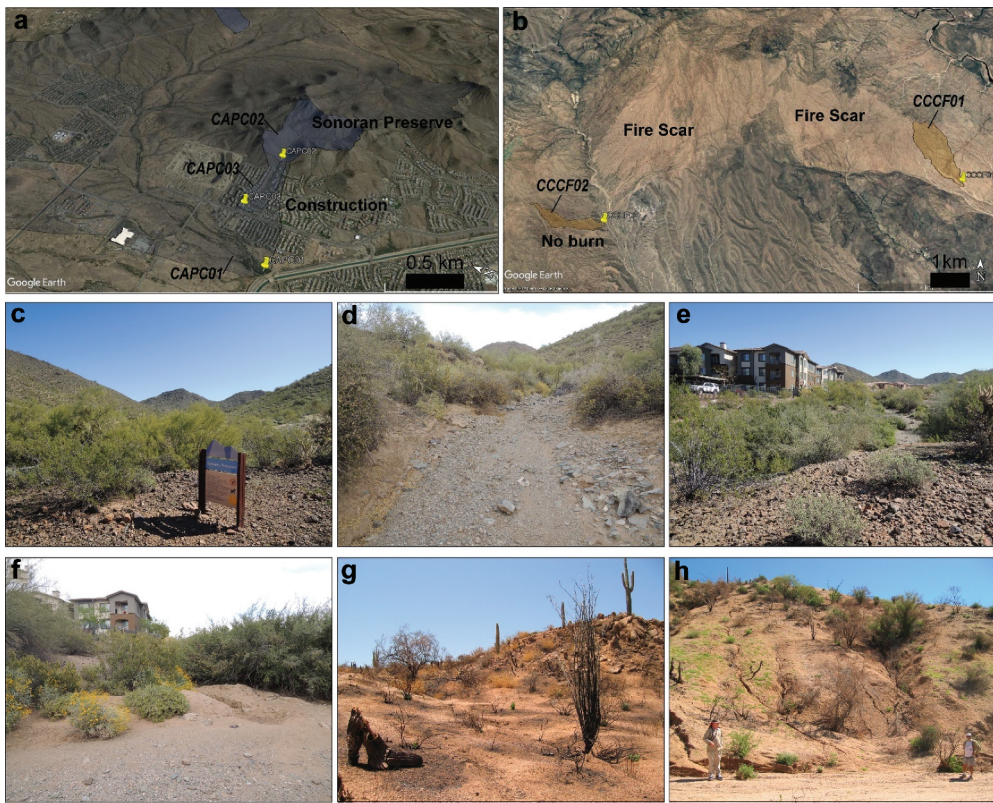
Figure 4. Study sites to test the key assumption that modern events do not modify catchment-averaged [10]Be denudation rates. (a) Google Earth view showing sampling locations and different land uses. The upper-subcatchment (CAPC02) within the Phoenix Sonoran preserve, while the lower-subcatchment (CAPC03) is highly disturbed by subdivision development. (b) CCCF01 catchment is within this burned area and CCCF02 is a controlled unburned catchment. (c, d) images of the natural CAPC02 catchment within the Phoenix Sonoran preserve contrast with images (e, f) showing the CAPC03 catchment disturbed by urban sprawl. (g) image of the 2005 Cave Creek complex Fire prior to any precipitation. (h) After the summer convective monsoon season, rills and meter-deep gullying was common in the burned area.

catchment-averaged [10]Be denudation rates in an arid region undergoing rapid urbanization (Jeong & Dorn, 2019, 2019), we felt it important to test the effects of both urbanization and wildfires generated by human activity on the urban fringe.

Figure 4 illustrates our experiment to test the impact of desert urban expansion on catchment-averaged [10]Be denudation rates analyzed previously (Jeong et al., 2021). In an idealized catchment, natural land cover occupies an upper-subcatchment and urban sprawl occupies the lower-subcatchment. Other controls on catchment-averaged [10]Be erosion rates, such as Early Proterozoic metavolcanic rock and a lack of mass wasting, remain similar. Land cover is the only variable to impact [10]Be catchment-averaged [10]Be denudation rates. We sampled an ideal site in 2016 (Figure 4a), collecting sediment samples from main stream (CAPC01), from the upper-subcatchment occupied by a desert preserve (CAPC02), and from lower sub-catchment that experienced

suburbanization within 2 years prior to sampling (CAPC03). Figure 4e & f provide insight about the detailed surface condition of the sampling locations.

The second set of experiment presented here for the first time was designed to examine the impacts of recent wildfire on catchment-averaged [10]Be erosion rates (Figure 4b). In 2005, the Cave Creek Complex fire burned about 1,000 km[2], which is one of the largest historic wildfires to burn Sonoran Desert (Allen et al., 2009). We collected sediment samples from a catchment in burned area (CCCF1), and in no-burnt area (CCCF2). Figure 4g & h provide insight into the detailed surface condition of the burned sites.

Mounds from animal burrowing

Commonly observed animals making mounds from burrowing in the study area include round tailed ground squirrel (*Xerospermophilus tereticaudus*), species of kangaroo rats (*Dipodomys* spp.), and pocket mice (*Perognathus* spp. and *Chaetodipus* spp.). These burrows occur under and around creosote bush (*Larrea tridentata*), brittle bush (*Encelia farinosa*), bursage (*Ambrosia deltoidea*), fairy duster (*Calliandra eriophylla*), and other small shrubs.

In order to understand the spatial abundance of these mounds, three line transects 100 m long were laid out across eleven stock pond catchments. First, the longest dimension of the stock pond catchment was located from lowest to highest elevation. Then, transects were laid out perpendicular to this longest dimension, located at 25%, 50%, and 75% of the total length of the longest dimension. The idea of this procedure was to randomize the placement of the transects in order to obtain an estimate of the area of sediment exposed by faunal burrowing. Where the transect tape intersected the mound material of an animal burrow, the length of the mound was recorded. The line transect method has a long tradition in vegetation sampling, providing an accurate estimate of the percent area of a plant species (Canfield, 1941). It similarly provides an estimate of percent area of exposed mounds from burrowing.

The timing of the measurement was in the dry period (typically between April and July) when frontal storms have ceased and the North American Monsoon has not started. These measurements were made in 1990 and repeated again in 1995. The abundance of housing construction activities or wildfire led to too much disturbance to continue this monitoring. This information has not been published previously, but was gathered as part of a long-term to monitor sediment erosion infilling stock ponds (cf. Jeong & Dorn, 2019).

Results

Catchment-averaged denudation rates in central Arizona

Catchment-averaged denudation rates for different locations in central Arizona vary between 5.3 and 76.9 m per million years (m My^{-1}). We note that m My^{-1} is the same value when portrayed as millimeters per thousand years (mm/ka). The mean catchment-averaged [10]Be denudation rate of the study area is 20.4 m My^{-1} and median rate is 17.6 m My^{-1} (Figure 5a). Catchment-averaged [10]Be denudation rates in the
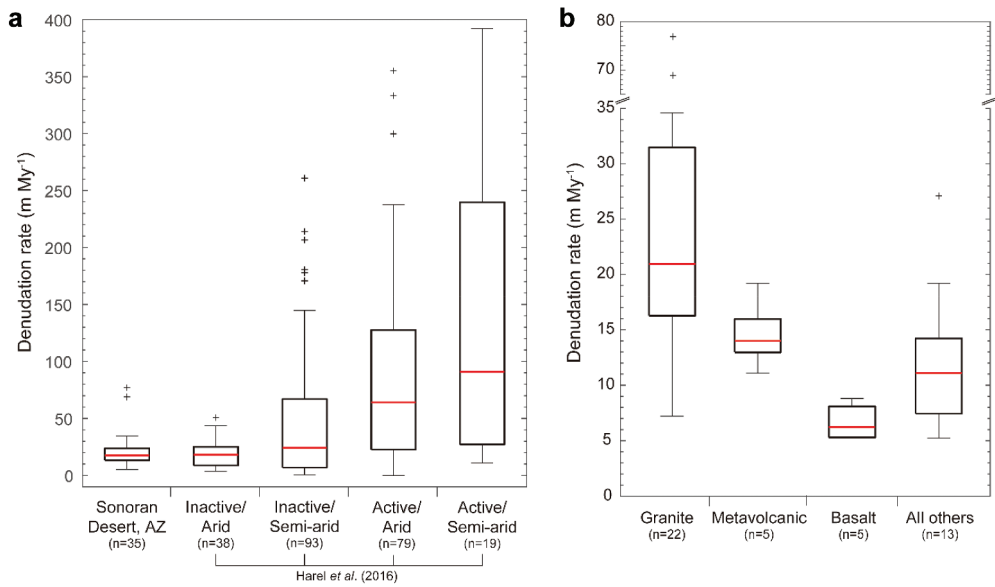
Figure 5. (a) box plots comparing [10]Be denudation rates in tectonically inactive Sonoran Desert with a global-scale [10]Be denudation analysis (Harel et al., 2016). We reclassified the global [10]Be denudation rate compilation (Harel et al., 2016) as climate (arid: MAP <250 mm, semi-arid: 250 mm≤MAP <500 mm) and tectonic activity (inactive: seismicity < 2 active: seismicity ≥ 2). Image a reproduced from Jeong et al. (2021). (b) the role of rock type on denudation in the northeast Sonoran Desert. Granitic watersheds dominated by sandy grus, and also located at the highest elevations, experience the highest erosion rates. Catchments that include basalt boulder and cobble-sized clasts experience the lowest erosion rates, but are also located at the lowest elevations. Those watersheds dominated by metavolcanic rocks rest between, as do catchments with a mixture of different rock types that lack basalt. "All others" are catchments that have a mix of non-granitic rock types, combining metavolcanic, basalt and ignimbrite.

tectonically inactive Sonoran Desert are statistically indistinguishable from rates previously published in arid inactive tectonic settings (Harel et al., 2016) (Figure 5a and Table S3).

Catchment-averaged [10]Be denudation rates of different rock types range from 7.2 to 76.9 m My^{-1} for granite, 5.2 to 8.8 m My^{-1} for basalt, 11.1 to 19.2 for m My^{-1} for metavolcanics (Figure 5a). The denudation rate in construction catchment (CAPC03) is within the external error of the denudation rate in preserve area (CAPC02). The catchment-averaged [10]Be denudation rates in burned area by 2005 Cave Creek Complex Fire (CCCF01) is also within the external error of the denudation rate in unburned area (CCCF02).

Statistical relationships between [10]Be denudation rate, elevation and precipitation in central Arizona

Catchment average slope, drainage area, and relief did not show a statistically significant relationship when compared with [10]Be-derived catchment averaged denudation rates (Table S2). Only mean elevation had a statistically significant linear correlation with [10]Be
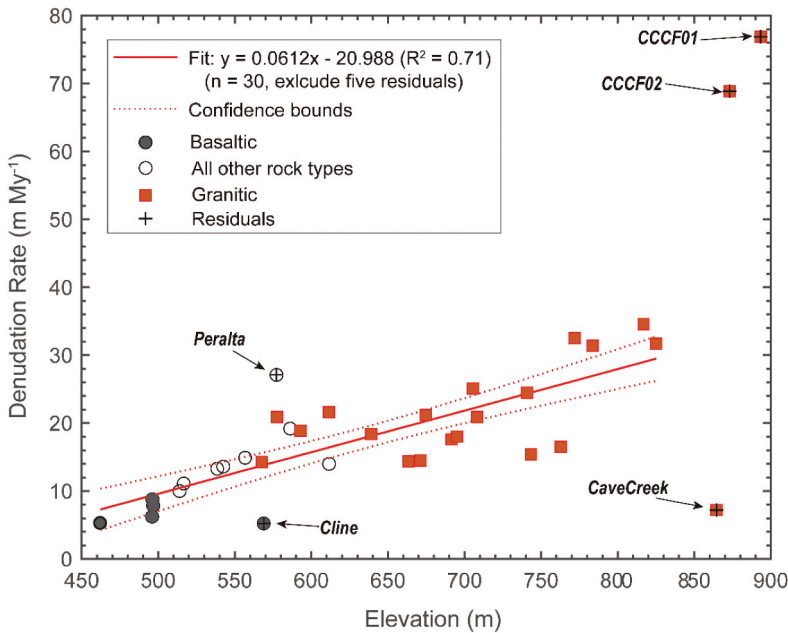
Figure 6. Scattergraph of all catchments comparing mean elevation and [10]Be erosion rate. The linear regression model also presented exclude the five identified outliers from the regression model. Since PIMA055/PIMA055a and PIMA056/PIMA056a were sampled in the exactly same catchments, averaged erosion rates were used.

erosion rate ($r = 0.69$, $p < 0.001$). The regression model between mean elevation and [10]Be erosion rate (Figure S1) explains 48% of the variation ($p < 0.00001$).

If the five outliers identified in Figure 6 are excluded, the regression model explains 71% of the relationship between erosion and elevation. Two outliers in Figure 6 are the Cave Creek Complex Fire sites (CCCF1 and CCCF2) that experienced much more extensive base-level lowering than any of the other sites. The Cave Creek and Peralta sites have very tiny catchment areas. The Cline site is the highest elevation catchment that also includes basalt boulders and cobbles. The discussion section explains potential reasons why it might be appropriate to remove these five different catchments from an elevation comparison. If these sites are discarded the p value drops to $p < 0.00000001$.

A separate set of linear regressions compared the mean elevation of all studied catchments: (i) with mean annual precipitation (MAP) (p-value <0.0001); (ii) with mean winter seasonal precipitation (MWSP) (p-value <0.0001); (iii) with the number of days when precipitation exceeded 25.4 mm (1 inch) (p-value = 0.0001); and (iv) with mean summer seasonal precipitation (MSSP) (p-value <0.05) (Figure 7). In all cases, but especially for cold-season precipitation (Figures 7b-c), higher elevations experienced more precipitation and more intense precipitation events.

Presence of basalt lowers [10]Be denudation rate

The boxplot in Figure 5b and the scatter graph in Figure 6 illustrates that catchments that include basalt clasts, typically small boulders and cobbles, have
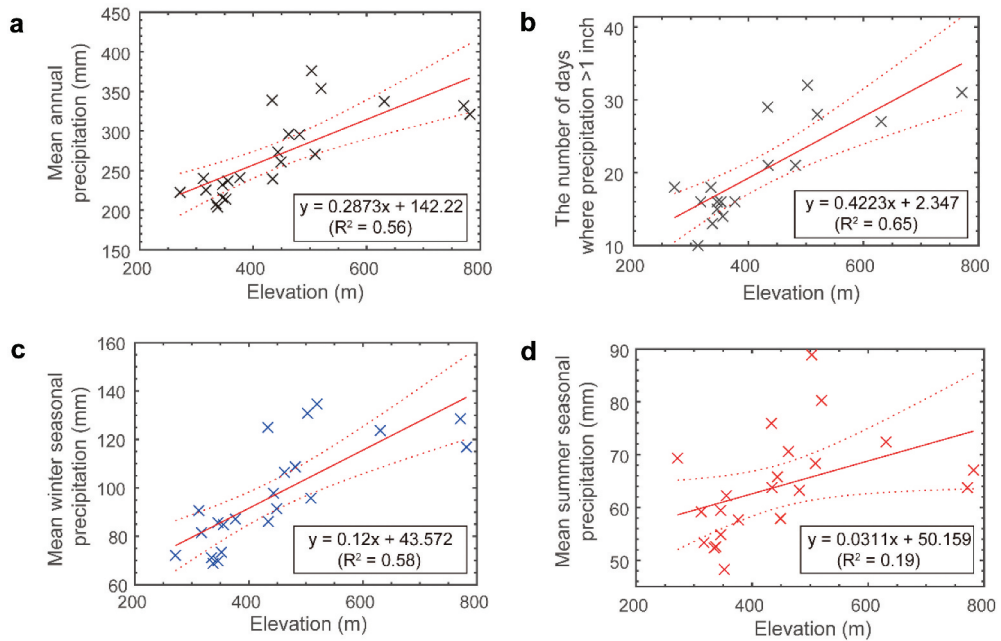
Figure 7. Regression model between precipitation variables and ^{10}Be erosion rate. (a) mean annual precipitation, (b) the number of days when precipitation exceeds 25.4 mm (1 inch), and (c) mean annual cold-season precipitation all have $p < 0.001$. Summer convective "monsoon" precipitation has a statistically significant correction with elevation at $p < 0.05$.

the lowest erosion rates. While these catchments are also found at the lowest elevations <500 m that are also the driest, the Cline catchment is above 550 m in elevation and it also exhibits the lowest denudation rate.

Mounds from animal burrowing

Table 2 reveals that higher elevation watersheds experienced a greater surface area of exposed mounding due to animal burrowing around perennial shrubs. This relationship holds true in both 1990 and 1995. When the average of all transect data gathered for a stock pond watershed is compared with mean elevation of that watershed, a statistically significant linear relationship exists with $p < 0.05$.

Two of the tanks were clearly anomalous in the amount of animal burrowing (Table 2), when considering the watershed elevation. The Peralta stock tank watershed had considerably higher percentage of watershed area with mounds exposed by animal burrowing, and the Cave Creek stock tank watershed had an anomalously low percentage, despite its higher elevation. The soil texture is a likely explanation. The Peralta tank soils had the highest amount of clay and silt in soils (82%) that aids burrowing, while the Cave Creek tank soils had the highest amount (61%) of coarse sand that makes burrowing much more difficult (Laundré & Reynolds, 1993).

Table 2. Percent area exposed to rainsplash and overland flow due to animal burrowing, based on three 100 m line transects with data gathered in 1990 and 1995.

Stock Pond Watershed	Mean Elevation(m) Watershed	Percent Exposure of Mound from Animal Burrowing Three transects (1,2,3) measured in 1990 and 1995						
		Tr1 90	Tr1 95	Tr2 90	Tr2 95	Tr3 90	Tr3 95	Ave ± SD
Cigar Tank	462	0.3	0.2	0.5	0.4	0.9	0.2	0.3 ± 0.2
Saguaro	496	0.2	0.1	0.4	0.5	0.2	0.1	0.3 ± 0.2
Bronco	497	0.2	0.2	0.2	0.2	0.4	0.3	0.3 ± 0.1
Gold Canyon	514	0.4	0.4	0.6	0.5	0.4	0.6	0.5 ± 0.1
Circle	538	0.5	0.4	0.5	0.4	0.4	0.6	0.5 ± 0.1
Peralta	577	1.3	1.2	1.1	1.5	1.1	0.7	1.2 ± 0.3
Asher Hills	671	0.6	0.5	0.7	0.7	0.6	0.7	0.6 ± 0.1
Buckhorn	743	0.7	0.7	0.6	0.6	0.9	0.8	0.7 ± 0.2
128th site 2	783	1.0	0.9	1.2	0.9	0.9	1.2	1.0 ± 0.1
Cave Creek*	865	0.0	*	0.2	*	0.6	*	0.3 ± 0.3

*This catchment was only surveyed in 1990, and not in 1995.

Discussion

Ruling out recent disturbance as an influence on [10]Be denudation rates

In order to employ catchment-averaged [10]Be denudation rates, investigators need to rule out the role of modern erosion for any new research setting. This is certainly the case for the Sonoran Desert. No prior research had confirmed that anthropogenic activities could not confound the interpretation of catchment-averaged [10]Be denudation rates as indicating natural erosion rates.

Rapid urbanization, wildfires, and cattle grazing in the Sonoran Desert have increased the region's vulnerability to erosion. Urbanization is often associated with paving over soils, but the processes of removing the vegetation and exposing bare ground for lengthy periods of time (Jeong, 2019; Jeong et al., 2018) led to increases in historic erosion rates (Jeong & Dorn, 2019). Humans have greatly enhanced wildfires in the area, starting with the invasion of exotic annual grasses such as *Bromus tectorum* and *Bromus madritensis ssp. Rubens* that altered natural grass/fire cycles (Brooks, 2008). For example, D'Antonio and Vitousek (1992) reported native shrublands replacement by invasive grasses produces abundant fine fuels followed by increasing frequency of large fires. Furthermore, after fires, invasive grasses typically thrive, leading to a fire regime that did not previously exist naturally (Brooks & Chambers, 2011). Biological soil crusts protecting desert surfaces from wind and water erosion (Allen, 2005; 2010) once settled extensively (Nagy et al., 2005), but currently remain only as patches – all due to human-induced disturbance such as cattle grazing (Jeong et al., 2018).

Although anthropogenic disturbances changed surface condition and accelerated historical erosion in the Sonoran Desert (Jeong & Dorn, 2019; Jeong et al., 2021), our new results reveal that the influence of historic events (i.e. wildfire, flooding, and housing development) on [10]Be denudation rates rests below the limit that we can detect (<10%) in the central Arizona. In other words, our results to test the anthropogenic impacts on catchment-averaged [10]Be denudation rates occur within the external error range of the method. Thus, catchment-averaged [10]Be denudation rates can be used to measure natural erosion rates in watersheds that do not

experience extensive landsliding, which is the case in this study. Future researchers should be aware that our conclusion would not apply in any locations where anthropogenic activity "mines" minerals below the cosmic ray penetration depth of ~60 cm.

Precipitation as a major control on Sonoran desert erosion: a key finding qualified

Our finding that catchment-averaged [10]Be denudation rates increase with elevation (Figure 6) is best explained by cold-season, frontal precipitation that increases with increasing elevation (Figure 7c). The study area of central Arizona has a particularly strong relationship between elevation and precipitation (Karnieli, 1990), because of an orographic effect (Bruintjes et al., 1994; Shinker & Bartlein, 2010). The strong elevation–precipitation relationship in the study area applies to both typical cold-season frontal storms that generate relatively gentle precipitation (Bruintjes et al., 1994) and also flood-producing winter atmospheric rivers (Hughes et al., 2014). While a slight positive relationship between elevation and summer precipitation also exists in the study area (Hawkins, 2003), the isolated nature of monsoonal storms means that summer thunder-storms are not as clearly tied to elevation (Figure 7d).

Our investigation into the relationship between study catchment elevation (a proxy for precipitation) and animal burrowing exposing mounds to rainsplash and overland flow must be considered. Surveys of the percent area in catchments with faunalturbation exposing bare ground reveal a strong connection with elevation. Higher elevation catchments with more precipitation (Figure 7c) have more faunalturbation, because food resources are more abundant for the round tailed ground squirrel (*Xerospermophilus tereticaudus*), species of kangaroo rats (*Dipodomys* spp), and pocket mice (*Perognathus* spp. and *Chaetodipus* spp.) (Stamp & Ohmart, 1978; Whitford & Kay, 1999).

Faunalturbation can generate new mound material, where individual mounds can exist for several years (Whitford & Kay, 1999). Although we did not measure modern erosion rates from mounds, rates in a Chilean study range from 0.34 m^3 ha^{-1} yr^{-1} in an arid setting to 0.56 m^3 ha^{-1} yr^{-1} in a semi-arid climate (Übernickel et al., 2021). These rates would be sufficient to influence [10]Be denudation rates, with the assumption that such mounds have occurred throughout the last 110 ka. No such insight exists at present, and hence we are left only with the reasonable possibility that some of the catchment-averaged [10]Be denudation precipitation signal results from an autocorrelation with faunalturbation.

The timescale of the catchment-averaged [10]Be denudation rates results ranges from ~8 ka in the most rapidly-eroding catchments to ca. 110 ka at the slowest-eroding sites (Table 1). This is the time period of the last major glacial-interglacial cycle. Unlike faunalturbation, prior research can address whether or not a precipitation gradient existed during the last glacial-interglacial cycle. This evidence comes from *Neotoma* packrat midden data that provides spatially specific insights into the nature of vegetation change in the study area for the last 40 ka. In contrast to pollen that integrates regional changes over a broad area, the big advantage of the packrat midden data is that the location of the fossil plant is constrained to the area of a few tends of meters around a *Neotoma* nest (Betancourt et al., 1990). Hence, it is possible to obtain some prior insight into how elevation influenced plant distributions in the past 40,000 years.

From the ~40 ka limit of radiocarbon to approximately 10 ka, *Neotoma*-based evidence indicates the study region experienced considerably cooler and wetter conditions (McAuliffe & Van Devender, 1998; Van Devender, 1990; Van Devender et al., 1987), where "late Wisconsin precipitation gradients were similar to those of today, with moisture increasing with elevation" (Van Devender et al., 1987, p. 346). For example, the sorts of juniper, pine and oak trees now found 1000 m higher occurred in the upper elevations of the study area mixed in with desert scrub.

The early Holocene from 10 to 8 ka appears to have been a time of transition with warming and drying, along with the onset of the summer monsoon rainfall ca 9–8 ka (McAuliffe & Van Devender, 1998, Weng and Jackson, 1999; Van Devender, 1990; Van Devender et al., 1987, 1987). The middle Holocene saw a slight increase in summer precipitation over modern conditions, and the modern climatic regime was established about 4 ka (Van Devender et al., 1987).

The region does not have good paleoclimatic records from ca. 100 ka to about 40 ka, during oxygen isotopes stages 5, 4 and early 3. However, nothing in the paleoclimatic record from oxygen isotope stages late 3, 2 or 1 would indicate anything other than an elevation-dependence of precipitation in the study area throughout the timescale of catchment-averaged ^{10}Be denudation rates. Our interpretation of the statistically significant (highly) relationship between catchment-averaged ^{10}Be denudation rates and elevation directly implies that increasing precipitation increases denudation in the northeastern Sonoran Desert.

There are also three other factors influencing the catchment-averaged ^{10}Be denudation rates data in Table 1 explored in the next three sections: rock type; base-level lowering; and sampling tiny drainage basins. However, accounting for these three non-climatic influences lends further support to the climatic interpretation presented here. If these sites explored in the sections are discarded from the regression of elevation versus denudation (Figure 6), the *p* value drops to p < 0.00000001.

Basalt as an influence on Sonoran desert ^{10}Be denudation rates

Figure 5 presents ^{10}Be erosion rates plotted against elevation (a proxy for precipitation) with symbols to indicate the rock types found in the watersheds. Most of the watersheds are underlain by granitic rocks, ranging from granite to gabbro, where the rock decay processes have produced mostly grus/sand. Four watersheds are underlain solely by metavolcanic rocks, where clast sizes on slopes are dominated by sizes ranging from cobbles to sand. The remainder of the watersheds mixes a variety of rock types.

The lowest erosion rates in the study are those watersheds that include basaltic clasts (e.g. Figure 2d). We note that the basalt clasts we observed are not mapped on geologic quadrangles, because the basic morphology of the lava flow has eroded away. All that is left of these ca. 24–16 Ma flows (Shafiqullah et al., 1980) are erosional remnants found armoring surfaces. The basalt found in the watersheds has either weathered to clay or consists of blocks with the smallest dimension greater than 30 cm.

Poesen et al. (1999) found that rock fragment cover reduces erosion rates associated with concentrated overland flow. The armoring effect of larger clasts is a complex topic with mixed signals with respect to the impact on erosion rates (Zhang et al., 2016). Generally, however, increasing rock fragments seem to reduce erosion, as reported in

laboratory Gong et al. (2018) and field (Dorn, 2015; Niu et al., 2019; von Bennewitz & Aladro, 2017; Xia et al., 2018) studies. Thus, the increased armoring associated with basalt blocks is likely part of the explanation for the lowest erosion rates, along with lower precipitation found at these lower elevation Sonoran Desert sites.

Base level drop increases ^{10}Be denudation rates

The base levels of all watersheds except CCCF1 and CCCF2 are either the Salt River or the Gila River (Figure 3). The ephemeral washes serving as local base levels for almost all of studied catchments display, at most, only a few meters of incision. In contrast, catchments CCCF1 and CCCF2 drain towards the Verde River (Figure 3). The relevant section of the Verde River experienced extensive base-level changes associated with its lake overflow and drainage integration history with substantial base level lowering in the Quaternary (Larson et al., 2020; Skotnicki et al., 2021). The net result is that the major ephemeral wash draining these two study sites incised more than 30 m in the Quaternary, and this wash serves as local base levels for CCCF1 and CCCF2. We speculate that the combination of higher precipitation and substantial local base-level drop led to these sites having the highest ^{10}Be denudation rates. Thus, we feel it would be inappropriate to include these sites in the elevation regression (Figure 6), where all of the other sites experienced an order of magnitude lower base-level decline in the Quaternary.

Anomalous erosion rates in small catchments: faunalturbation or a superstorm?

Two very small catchment sites stand out as outliers in the elevation regression: Cave Creek and Peralta (Table 1 and Figure 6). These catchments also stand out as outliers in exposure of faunalturbation mounds (Table 2). Peralta at a low elevation has an anomalously high ^{10}Be denudation rate of 27.1 ± 1.7 mm/ka, and Cave Creek at a high elevation has an anomalously low ^{10}Be denudation rate of 7.2 ± 0.5 mm/ka. We have no good explanation, based on drainage basin characteristics, why the Cave Creek catchment should have such a low denudation rate and why the Peralta catchment should have such a high denudation rate for their respective elevations.

As noted earlier, Peralta has a lot of clay and silt in the soil, favorable for animal burrowing (Laundré & Reynolds, 1993). Cave Creek has an anomalous concentration of coarse sand in the soil, which is unfavorable for animal burrowing in the Sonoran Desert (Laundré & Reynolds, 1993). Thus, the cause of the catchment-averaged ^{10}Be denudation rate anomaly could be particularly high or low concentrations of animal burrows exposing bare ground to rainsplash or overland flow.

We also think that it is possible that an external factor such as a superstorm might explain these anomalies, "hitting" Peralta and "missing" Cave Creek. This is highly speculative, but there is some evidence to suggest the possible role of a high-magnitude and low-frequency event. We note that very small catchments could be susceptible to the effect of convective superstorms that are 10,000 to 1000-year events of the sort discussed by Schick and Magid (1978). Hawkins (2003) studied summer monsoon storms in the study area and confirmed that any given convective cell's location, when it "lets loose" with its most intense precipitation, is somewhat random. There are two speculative inferences that could be made in the interpretation of ^{10}Be denudation rates in tiny

catchments: (i) the likelihood of a superstorm "hitting" these tiny areas is lower than a superstorm impacting a larger area; (ii) a superstorm that "hits" a tiny catchment would have an erosive effect on the ^{10}Be denudation rate that is inversely proportional to drainage area.

We illustrate the idea behind this speculation that a "superstorm" hitting an entire tiny catchment could increase catchment-averaged ^{10}Be denudation rates much more than such a storm hitting a portion of a larger catchment. In this illustration, we observed the effect of one such superstorm in the 1.3 km^2 Hawes watershed (Figure 8a), that led to over 5 m of downcutting at some point in the past and transported metavolcanic boulders >2 m in the long axis downstream (Figure 8b).

The broader catchment-averaged ^{10}Be denudation rate literature includes analyses of small drainages. Granger et al. (1996) used very small catchments above the shorelines of late Pleistocene Lake Lahontan to test the catchment-averaged ^{10}Be method, where the accumulating alluvial fan buried lacustrine shorelines of known age. The Lake Lahontan area of northwest Nevada does experience summer monsoon thunderstorms, but at a frequency much lower than the Mojave Desert of eastern California Harvey et al. (1999) and even lower than the study area (Hawkins, 2003).

In summary, while the removal of the anomalous catchment-averaged ^{10}Be denudation rates in these two tiny catchments from the regression in Figure 6 increases the statistical significance of the elevation- catchment-averaged ^{10}Be denudation rates relationship slightly, this section's greater significance rests in the need for greater scrutiny of catchment-averaged ^{10}Be denudation rates in tiny arid catchments and their relationship to zoo geomorphic processes and high magnitude precipitation events.

Re-visiting the arid/semi-arid part of Langbein and Schumm's erosion curve with ^{10}Be denudation rates

A 60-year debate over the impact of climate on erosion (see Figure 1 in Riebe et al., 2001; Langbein & Schumm, 1958), including global-scale syntheses of catchment-averaged ^{10}Be denudation rates, has not found a clear correlation between denudation and precipitation (Harel et al., 2016; Portenga & Bierman, 2011; von Blanckenburg, 2005; Willenbring et al., 2013), perhaps because tectonically linked variables such as slope swamp any precipitation signal. Here, we eliminate any tectonic effects by studying erosion in the quiescent Sonoran Desert.

Our finding that catchment-averaged ^{10}Be denudation rates yield natural background rates of erosion over timescales of 10^3-10^5 years in a setting lacking any significant tectonics during the residence time of ^{10}Be may have allowed us to detect a clearer precipitation signal than others have seen. Another possible reason why we detected a clear precipitation signal is the presence of the same orographic gradient during the late Quaternary, as determined by *Neotoma* packrat midden studies done in the Sonoran Desert. We note that a positive relationship between precipitation and denudation rates has also been reported in the central Atacama Desert Placzek et al. (2014) and the Anti-Atlas of Morocco (Clementucci et al., 2022), and in a recent analysis of global ^{10}Be denudation data (Ruetenik et al., 2022).

Langbein and Schumm's (1958) model hypothesized that the distribution of erosion rates by climate is right-skewed, with the lowest erosion rates in arid climates, maximum
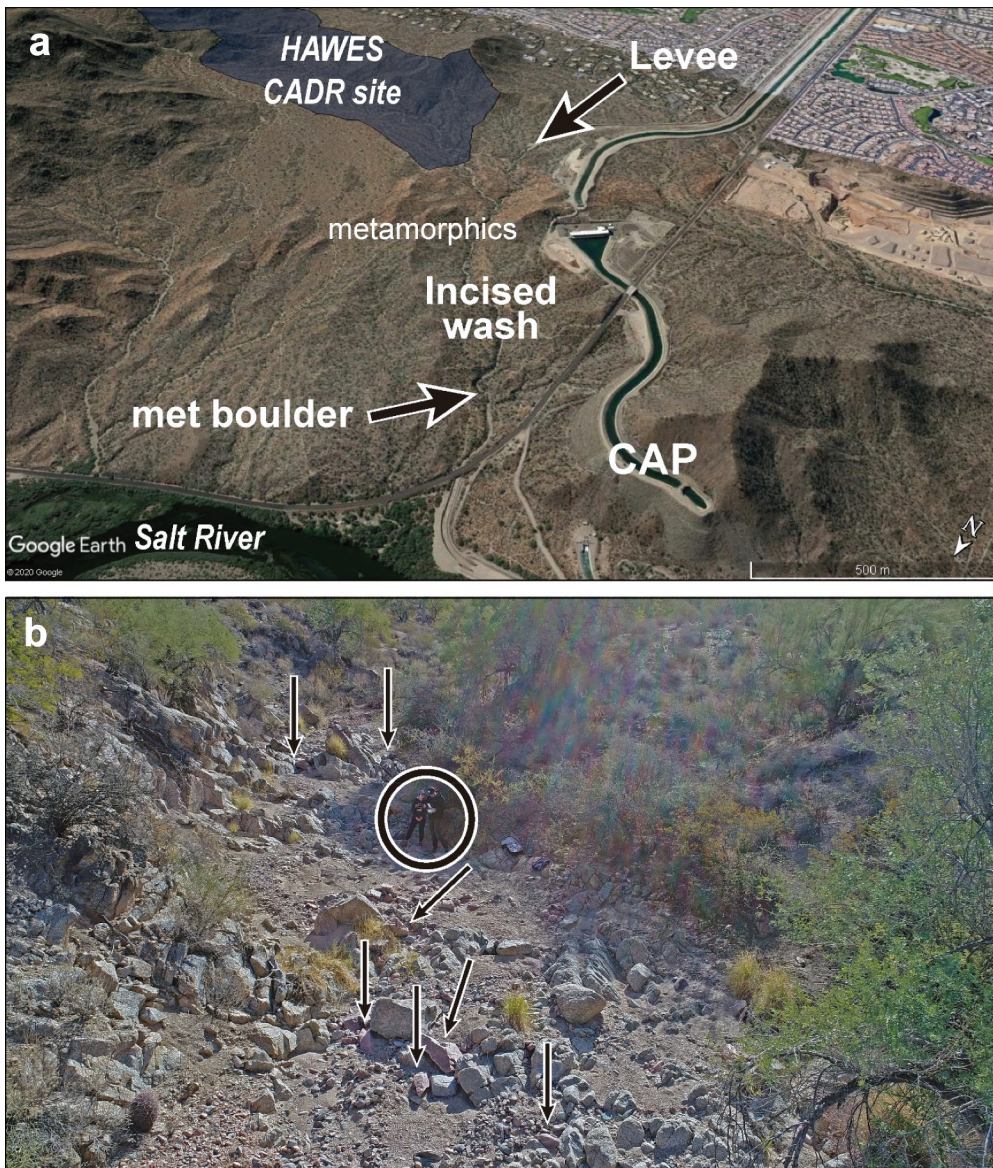
Figure 8. (a) a study site nears the Hawes catchment-averaged [10]Be denudation rates catchment where we observed the effect of a paleo-superstorm. The Google Earth image shows a levee built to protect the central Arizona Project (CAP) canal that redirected runoff from housing subdivisions into a small desert wash. The anthropogenic incision that resulted exposed >2 m boulders that had been moved in when the wash experienced a superstorm sometime in the past. (b) Drone scanning images of the study site. At the lower reach of the HAWES catchments, metavolcanic boulders likely delivered by superstorm are observed (note humans for scale). In contrast, similarly sized boulders used by the CAP to inhibit erosion were not transported by the incision-generating flooding.

rates in semi-arid environments, followed by a decline of erosion in wetter places due to heightened vegetation cover (Figure 9). Our catchment-averaged [10]Be denudation rate data from catchments with mean elevations from 460 to 890 m (ca. MAP ranges from 262 to 384 mm) reveal statistically significant increases with increasing elevation, and this relationship fits to the arid/semi-arid part of Langbein and Schumm's erosion curve. Research by Schaller and Ehlers (2022) in the Chilean Coastal Cordillera also shows increasing cosmogenic denudation rates between 0 and 400 mm MAP. However, our data (when Langbein and Schumm's units are converted to m/Ma) reveal considerably lower erosion rates than those plotted in 1958.

In a speculative exercise, we combined our data with another Arizona catchment-averaged [10]Be denudation rates data set studying higher and much wetter elevations in Arizona and also in a location dominated by summer precipitation. In the Pinaleño Mountains (ca. MAP ranges from 653 to 964 mm denudation rates decrease with increasing elevations (Jungers & Heimsath, 2016). Despite a weak relationship, Jungers and Heimsath's (2016) data fit the wetter part of Langbein and Schumm's erosion curve when combined with our data (Figure 9). The decline seen at higher precipitation levels could be explained by the greater vegetation cover at higher elevations in southeastern
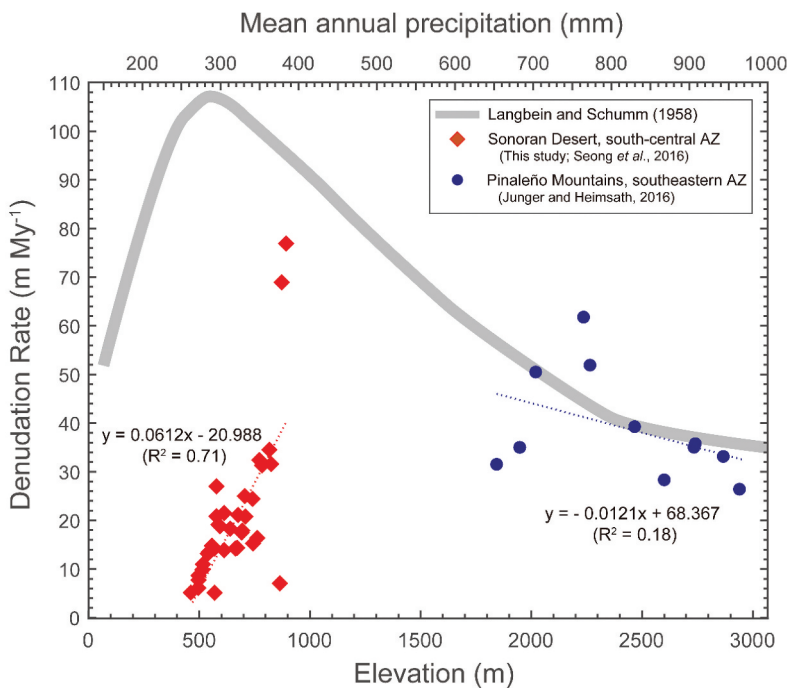

Figure 9. Scatter graph and linear regression of available [10]Be denudation rate from Arizona, USA. The grey curve presents a classic theory postulating a link between climate and erosion (Langbein & Schumm, 1958) where maximum erosion occurs in a semi-arid climate, lowering with less precipitation and more vegetation cover. The positive relationship between elevation and denudation rate in arid/semi-arid region (lower elevation), and negative relationship in wetter region (higher elevation) fit the Langbein and Schumm's (1958) curve. Mean annual precipitation was calculated from simple regression between elevation and mean annual precipitation using normal data 73 meteorological stations of NOAA U.S. annual climate normals (1981–2010) (Arguez et al., 2010).

Arizona (Van Leeuwen et al., 2010). In summary of this section, our analysis here supports Mishra et al. (2019)'s conclusion that both precipitation and vegetation play an important role in geomorphic denudation.

Conclusion

Langbein and Schumm (1958) first proposed that erosion rates increase from extremely arid to semiarid conditions, peaking at about 300 mm of mean annual precipitation, and then decline with increasing humidity as vegetation cover increases. Their curve has seen widespread use in physical geography, geomorphology, soil science, and physical geology textbooks for the past half-century. Prior [10]Be-based denudation research on the impact of climate on long-term erosion rates typically does not see a strong correlation with precipitation, but instead stresses the role of tectonics as a major driver on erosion rates (Harel et al., 2016; Portenga & Bierman, 2011; von Blanckenburg, 2005; Willenbring et al., 2013). Still, some [10]Be-based denudation research (Adams et al., 2020; Clementucci et al., 2022; Mishra et al., 2019; Ruetenik et al., 2022) did find some level of precipitation control on erosion.

This first systematic study of the influence of precipitation on catchment-averaged [10]Be denudation rates in a North American desert is set in the northeastern Sonoran Desert, Arizona, USA. This region, surrounding metropolitan Phoenix, hosts a highly statistically significant modern precipitation gradient driven by an orographic effect associated with increasing elevation. A statistically significant modern precipitation gradient also occurs in the summer monsoon season, albeit to a much lesser extent. With the timescale of our catchment-averaged [10]Be denudation rate data ranging from 8 to 113 ka, it is important to emphasize that the Sonoran Desert has been the subject of extensive paleoclimatic research over the last 40,000 years, based on the study of *Neotoma* packrat middens, and this same elevation-dependent increase in precipitation appears to have been in place throughout the late Pleistocene and Holocene. Also, with no significant tectonic activity in the last 2.5 Ma (Skotnicki et al., 2021), the northeastern Sonoran Desert provides a unique study region to assess the arid/semiarid limb of Langbein and Schumm's (1958) classic erosion curve.

Our primary research finding is that catchment-averaged [10]Be denudation rates have a statistically significant relationship with increasing elevation, and hence precipitation appears to be a primary driving factor in this tectonically quiescent Sonoran Desert setting. A plot of our data on Langbein and Schumm's (1958) curve suggests that erosion peaks in slightly wetter catchments than those found over six decades ago.

Another major finding is that zoogeomorphic activity in the form of faunalturbation exposing bare soil to rainsplash and overland flow is likely also involved in controlling erosion, in that more faunalturbation occurs in higher elevation study catchments. The role of zoogeomorphic activity on long-term catchment-averaged [10]Be denudation rates and its possible autocorrelation with precipitation is not a typical component of [10]Be denudation scholarship on the role of climate; we think it should be considered more often.

A third finding involves negative conclusions, identifying factors that do not influence [10]Be denudation rates in the Sonoran Desert. A statistical analysis of our catchments revealed no connections between catchment-averaged [10]Be denudation rates and slope,

drainage area, relief, or whether the catchment was found on a pediment, alluvial fan or entirely within a range. We also found that urbanization and wildfire events, that can greatly increase historic erosion in the Sonoran Desert (Jeong & Dorn, 2019), had no impact on [10]Be denudation rate. The only statistically significant control on catchment-averaged [10]Be denudation rate appears to be elevation, which is a surrogate for precipitation in our study region.

A fourth finding is similar to Duxbury et al. (2015)'s study of [10]Be denudation rates in the much wetter climate of Virginia, USA, that rock type can be an important control on erosion. In the Sonoran Desert, the presence of basalt boulders and cobbles appears to provide an armoring effect that decreases erosion rates.

A fifth finding is that substantial base-level lowering can mimic the effect of tectonics in increasing [10]Be denudation rates in the Sonoran Desert. While study region is tectonically quiet (Skotnicki & DePonty, 2020; Skotnicki et al., 2021), drainage integration of the Verde River about 2.5 Ma (Skotnicki et al., 2021) led to substantial base level lowering in two watersheds that had catchment-averaged [10]Be denudation rates about 3× higher than what would be expected for the elevation of these sites. Our interpretation of this base-level drop of the catchment's trunk stream mimics the increase in fluvial relief provided by tectonic uplift (cf. Adams et al., 2020).

Geomorphology is a field undergoing vast changes, due to innovations in the use of cosmogenic nuclides and increasingly due to machine learning (Houser et al., 2022). In fact, there is a possibility that cosmogenic nuclide analyses of erosion rates like those presented here could be translated via process-based numerical models (cf. Houser et al., 2022). Hence, all authors on this paper believe strongly that a deep field understanding must come first prior to any extrapolation via machine learning or numerical modeling; a failure to appreciate the field could easily result in overinterpreting findings such as those presented here.

Highlights

- Rainfall is a key factor eroding catchments in a tectonically calm desert
- The classic Langbein and Schumm's erosion curve fits our arid/semiarid [10]Be data
- Animal burrowing, rock type and tiny catchment size influence [10]Be data
- Big drops in base-level mimic tectonics in increasing erosion rates
- [10]Be denudation rates insensitive to construction and wildfire in the Sonoran Desert

Acknowledgments

Disclosure statement

ORCID

Ara Jeong 🔟 http://orcid.org/0000-0002-0177-1187
Yeong Bae Seong 🔟 http://orcid.org/0000-0001-6605-3912
Ronald I. Dorn 🔟 http://orcid.org/0000-0003-1343-4556
Byung Yong Yu 🔟 http://orcid.org/0000-0001-8058-5288

Data availability statement

The authors confirm that the data supporting the findings of this study are available within the article and its supplementary materials.

References

Adams, B. A., Whipple, K. X., Forte, A. M., Heimsath, A. M., & Hodges, K. V. (2020). Climate controls on erosion in tectonically active landscapes. *Science Advances*, 6(42), eaaz3166. https://doi.org/10.1126/sciadv.aaz3166

Allen, C. D. (2005). Micrometeorology of a smooth and rugose biological soil crust near Coon Bluff, Arizona. *Journal of the Arizona-Nevada Academy of Science*, 21–28. https://www.jstor.org/stable/27641735

Allen, C. D. (2010). Biogeomorphology and biological soil crusts: a symbiotic research relationship. *Géomorphologie: relief, processus, environnement*, 16(4), 347–358. https://doi.org/10.4000/geomorphologie.8071

Allen, C. D., Dorn, J. D., & Dorn, R. I. (2009). Fire in the Desert: Initial gullying associated with the Cave Creek complex Fire, Sonoran Desert, Arizona. *Yearbook of the Association of Pacific Coast Geographers*, 71(1), 182–195. https://doi.org/10.1353/pcg.0.0033

Arguez, A., Durre, I., Applequist, S., Squires, M., Vose, R., Yin, X., & Bilotta, R. (2010). NOAA's U.S. Climate normals (1981-2010). NOAA National Centers for Environmental information. Retrieved December 9th, 2020, from https://doi.org/10.7289/V5PN93JP

Balco, G., Stone, J. O., Lifton, N. A., & Dunai, T. J. (2008). A complete and easily accessible means of calculating surface exposure ages or erosion rates from 10Be and 26Al measurements. *Quaternary geochronology*, 3(3), 174–195. https://doi.org/10.1016/j.quageo.2007.12.001

Betancourt, J. L., Van Devender, T. R., & Martin, P. S. (Eds.). (1990). *Packrat middens: The last 40,000 years of biotic change*. University of Arizona Press.

Brooks, M. L., 2008. Plant invasions and fire regimes. Zouhar, K., Smith, J. K., Sutherland, S., Brooks, M. L. Plant invasions and fire regimes. Wildland fire in ecosystems, fire and nonnative invasive plants Ogden, UT, USA US Department of Agriculture, Forest Service, RMRS-GTR -42-, 6:33–45

Brooks, M. L., & Chambers, J. C. (2011). Resistance to invasion and resilience to fire in desert shrublands of North America. *Rangeland Ecology & Management*, 64(5), 431–438. https://doi.org/10.2111/REM-D-09-00165.1

Bruintjes, R. T., Clark, T. L., & Hall, W. D. (1994). Interactions between topographic airflow and cloud/precipitation development during the passage of a winter storm in Arizona. *Journal of the Atmospheric Sciences*, 51(1), 48–67. https://doi.org/10.1175/1520-0469(1994)051<0048:IBTAAC>2.0.CO;2

Butler, D. R. (1995). *Zoogeomorphology: Animals as geomorphic agents*. Cambridge University Press.

Canfield, R. H. (1941). Application of the line interception method in sampling range vegetation. *Journal of Forestry*, 39(4), 388–394. https://doi.org/10.1093/jof/39.4.388

Cavin, R. M., & Butler, D. R. (2015). Patterns and trends in the fields of bioturbation, faunalturbation, and zoogeomorphology. *Physical Geography*, 36(3), 178–187. https://doi.org/10.1080/02723646.2015.1026763

Chapman, A. D., Rautela, O., Shields, J., Ducea, M. N., & Saleeby, J. (2019). Fate of the lower lithosphere during shallow-angle subduction: The Laramide example. *GSA Today*, *30*(1), 4–10. https://doi.org/10.1130/GSATG412A.1

Clementucci, R., Ballato, P., Siame, L. L., Faccenna, C., Yaaqoub, A., Essaifi, A., Laëtitia, L., & Guillou, V. (2022). Lithological control on topographic relief evolution in a slow tectonic setting (Anti-Atlas, Morocco). *Earth and Planetary Science Letters*, *596*, 117788. https://doi.org/10.1016/j.epsl.2022.117788

Coggan, N. V., Hayward, M. W., Gibb, H., & Rodriguez-Cabal, M. (2018). A global database and "state of the field" review of research into ecosystem engineering by land animals. *Journal of Animal Ecology*, *87*(4), 974–994. https://doi.org/10.1111/1365-2656.12819

Covault, J. A., Craddock, W. H., Romans, B. W., Fildani, A., & Gosai, M. (2013). Spatial and temporal variations in landscape evolution: Historic and longer-term sediment flux through global catchments. *The Journal of Geology*, *121*(1), 35–56. https://doi.org/10.1086/668680

D'Antonio, C. M., & Vitousek, P. M. (1992). Biological invasions by exotic grasses, the grass/fire cycle, and global change. *Annual Review of Ecology and Systematics*, *23*(1), 63–87. https://doi.org/10.1146/annurev.es.23.110192.000431

Dirks, P. H. G. M., Placzek, C. J., Fink, D., Dosseto, A., & Roberts, E. (2016). Using 10Be cosmogenic isotopes to estimate erosion rates and landscape changes during the plio pleistocene in the cradle of humankind, South Africa. *Journal of Human Evolution*, *96*, 19–34. https://doi.org/10.1016/j.jhevol.2016.03.002

Dorn, R. I. (2015). Impact of consecutive extreme rainstorm events on particle transport: Case study in a Sonoran Desert range, western USA. *Geomorphology*, *250*, 53–62. https://doi.org/10.1016/j.geomorph.2015.08.017

Duxbury, J., Bierman, P. R., Portenga, E. W., Pavich, M. J., Southworth, S., & Freeman, S. P. H. T. (2015). Erosion rates in and around Shenandoah National Park, Virginia, determined using analysis of cosmogenic [10]Be. *American Journal of Science*, *315*(1), 46–76. https://doi.org/10.2475/01.2015.02

Eaton, G. P. (1982). The basin and range province: Origin and tectonic significance. *Annual Review of Earth and Planetary Sciences*, *10*(1), 409–440. https://doi.org/10.1146/annurev.ea.10.050182.002205

Gellis, A. C., Pavich, M. J., Bierman, P. R., Clapp, E. M., Ellevein, A., & Aby, S. (2004). Modern sediment yield compared to geologic rates of sediment production in a semi- arid basin, 32 New Mexico: Assessing the human impact. *Earth Surface Processes and Landforms*, *29*(11), 1359–1372. https://doi.org/10.1002/esp.1098

Gong, T., Zhu, Y., & Shao, M. (2018). Effect of embedded-rock fragments on slope soil erosion during rainfall events under simulated laboratory conditions. *Journal of Hydrology*, *563*, 811–817. https://doi.org/10.1016/j.jhydrol.2018.06.054

González, C., Kelley, M., Marvin, M. C., López-Castañeda, N., Dorn, R. I., & Schmeeckle, M. (2022). Regional piedmont incision during base-level rise in the northeastern Sonoran Desert, Arizona, USA. *Physical Geography*, *43*(1), 67–97. https://doi.org/10.1080/02723646.2021.1934964

Gootee, B. F. (2013). An evaluation of carbon dioxide sequestration potential in the Higley basin, south-central Arizona. Arizona geological survey open file report OFR-. map plates and 2 appendices *13-10*, 14 p., 6.

Granger, D. E., Kirchner, J. W., & Finkel, R. (1996). Spatially averaged long-term erosion rates measured from in situ-produced cosmogenic nuclides in alluvial sediment. *The Journal of Geology*, *104*(3), 249–257. https://doi.org/10.1086/629823

Granger, D. E., & Schaller, M. (2014). Cosmogenic nuclides and erosion at the watershed scale. *Elements*, *10*(5), 369–373. https://doi.org/10.2113/gselements.10.5.369

Harel, M.-A., Mudd, S. M., & Attal, M. (2016). Global analysis of the stream power law parameters based on worldwide 10Be denudation rates. *Geomorphology*, *268*, 184–196. https://doi.org/10.1016/j.geomorph.2016.05.035

Harvey, A. M., Wigand, P. E., & Wells, S. G. (1999). Response of alluvial fan systems to the late Pleistocene to Holocene climatic transition: Contrasts between the margins of pluvial lakes

Lahontan and Mojave Nevada and California, USA. *Catena*, *36*(4), 255–281. https://doi.org/10. 1016/S0341-8162(99)00049-1

Hawkins, T. W. (2003). Geostatistical analysis of Arizona summertime precipitation. *Journal of the Arizona-Nevada Academy of Science*, *36*(1), 9–17. https://www.jstor.org/stable/40022387

Hembree, D. I., Smith, J. J., Buynevich, I. V., & Platt, B. F. (2017). Neoichnology of semiarid environments: Soils and burrowing animals of the Sonoran Desert, Arizona, USA. *Palaios*, *32* (9), 620–638. https://doi.org/10.2110/palo.2017.009

Houser, C., Lehner, J., & Smith, A. (2022). The field geomorphologist in a time of artificial intelligence and machine learning. *Annals of the American Association of Geographers*, *112*(5), 1260–1277. https://doi.org/10.1080/24694452.2021.1985956

Hughes, M., Mahoney, K. M., Neiman, P. J., Moore, B. J., Alexander, M., & Ralph, F. M. (2014). The landfall and inland penetration of a flood-producing atmospheric river in Arizona. Part II: Sensitivity of modeled precipitation to terrain height and atmospheric river orientation. *Journal of Hydrometeorology*, *15*(5), 1954–1974. https://doi.org/10.1175/JHM-D-13-0176.1

Jeong, A. (2019). Sediment accumulation expectations for growing desert cities: A realistic desired outcome to be used in constructing appropriately sized sediment storage of flood control structures. *Environmental Research Letters*, *14*(12), 125005. https://doi.org/10.1088/1748-9326/ab30e5

Jeong, A., Cheung, S. Y., Walker, I. J., & Dorn, R. I. (2018). Urban geomorphology of an arid city: Case study of Phoenix, Arizona. In M. J. Thornbush (Ed.), *Urban geomorphology: Landforms and processes in cities* (pp. 175–204). Elsevier. https://doi.org/10.1016/B978-0-12-811951-8. 00010-2

Jeong, A., & Dorn, R. I. (2019). Soil erosion from urbanization processes in the Sonoran Desert, Arizona, USA. *Land Degradation & Development*, *30*(2), 226–238. https://doi.org/10.1002/ldr. 3207

Jeong, A., Dorn, R. I., Seong, Y. B., & Yu, B. Y. (2021). Acceleration of soil erosion by different land uses in arid lands above 10Be natural background rates: Case study in the Sonoran Desert, USA. *Land*, *10*(8), 834. https://doi.org/10.3390/land10080834

Jeong, A., Lee, J. I., Seong, Y. B., Balco, G., Yoo, K.-C., Yoon, H. I., Domack, E., Rhee, H. H., & Yu, B. Y. (2018). Late Quaternary deglacial history across the Larsen B embayment, Antarctica. *Quaternary Science Reviews*, *189*, 134–148. https://doi.org/10.1016/j.quascirev.2018.04.011

Jungers, M. C., & Heimsath, A. M. (2016). Post-tectonic landscape evolution of a coupled basin and range: Pinaleño Mountains and Safford basin, southeastern Arizona. *Geological Society of America Bulletin*, *128*(3–4), 469–486. https://doi.org/10.1130/B31276.1

Karnieli, A. (1990). Application of kriging technique to areal precipitation mapping in Arizona. *GeoJournal*, *22*(4), 391–398. https://doi.org/10.1007/BF00174760

Kim, D. E., Seong, Y. B., Byun, J., Weber, J., & Min, K. (2016). Geomorphic disequilibrium in the eastern Korean Peninsula: Possible evidence for reactivation of a rift-flank margin. *Geomorphology*, *254*, 130–145. https://doi.org/10.1016/j.geomorph.2015.11.022

Kim, D. E., Seong, Y. B., Weber, J., & Yu, B. Y. (2022). Frost-weathering control on the rate of late Quaternary landscape evolution, western flank of the Taebaek Mountain range, Korea: A case of passive margin landscape evolution. *Geografiska Annaler, Series A: Physical Geography*, *104*(4), 1–23. https://doi.org/10.1080/04353676.2022.2121998

Kirchner, J. W., Finkel, R. C., Riebe, C. S., Granger, D. E., Clayton, J. L., King, J. G., & Megahan, W. F. Mountain erosion over 10 yr, 10 k.Y., and 10 m.Y. time scales. (2001). *Geology*, *29*(7), 591–594. (2001)0292.0.CO;2. https://doi.org/10.1130/0091-7613(2001) 029<0591:MEOYKY>2.0.CO;2

Kohl, C. P., & Nishiizumi, K. (1992). Chemical isolation of quartz for measurement of in-situ-produced cosmogenic nuclides. *Geochimica et cosmochimica acta*, *56*(9), 3583–3587. https://doi. org/10.1016/0016-7037(92)90401-4

Langbein, W. B., & Schumm, S. A. (1958). Yield of sediment in relation to mean annual precipitation. *Transactions American Geophysical Union*, *39*(6), 1076–1084. https://doi.org/10. 1029/TR039i006p01076

Larson, P. H., Dorn, R. I., Skotnicki, S. J., Seong, Y. B., Jeong, A., & DePonty, J. (2020). Impact of drainage integration on basin geomorphology and landform evolution: A case study along the Salt and Verde rivers, Sonoran Desert, USA. *Geomorphology*, *369*, 107439. https://doi.org/10.1016/j.geomorph.2020.107439

Laundré, J. W., & Reynolds, T. D. (1993). Effects of soil structure on burrow characteristics of five small mammal species. *The Great Basin Naturalist*, *53*(4) , 358–366. https://www.jstor.org/stable/41712798

Lee, J. A. (1986). Origin of mounds under creosote bush (Larrea tridentata) on terraces of the Salt river, Arizona. *Journal of the Arizona-Nevada Academy of Science*, *21*(1) , 23–28. https://www.jstor.org/stable/40026003

Lee, C.-H., Seong, Y. B., Schoenbohm, L. M., Kim, D.-E., & Yu, B. Y. (2021). Geomorphic constraints on the development of a blind-thrust induced landform, south-central Mongolia: Insights into foreberg growth. *Geomorphology*, *378*, 107613. https://doi.org/10.1016/j.geomorph.2021.107613

Leighty, R. S., Skotnicki, S. J., & Pearthree, P. A. 000. (1997). Geologic map of the Cave Creek Quadrangle, Maricopa County, Arizona. Arizona Geological Survey Open File Report, OFR-97-01, 2 map sheets, map scales. *1*(241), 12,000, 38.

Lifton, N., Sato, T., & Dunai, T. J. (2014). Scaling in situ cosmogenic nuclide production rates using analytical approximations to atmospheric cosmic-ray fluxes. *Earth and Planetary Science Letters*, *386*, 149–160. https://doi.org/10.1016/j.epsl.2013.10.052

McAuliffe, J. R., & Van Devender, T. R. (1998). A 22,000-year record of vegetation change in the north-central Sonoran Desert. *Palaeogeography, Palaeoclimatology, Palaeoecology*, *141*(3–4), 253–275. https://doi.org/10.1016/S0031-0182(98)00054-6

Mishra, A. K., Placzek, C., Jones, R., & Zerboni, A. (2019). Coupled influence of precipitation and vegetation on millennial-scale erosion rates derived from 10Be. *PLoS One*, *14*(1), e0211325. https://doi.org/10.1371/journal.pone.0211325

Montgomery, D. R. (1999). Process domains and the river continuum 1. *JAWRA Journal of the American Water Resources Association*, *35*(2), 397–410. https://doi.org/10.1111/j.1752-1688.1999.tb03598.x

Nagy, M. L., Pérez, A., & Garcia-Pichel, F. (2005). The prokaryotic diversity of biological soil crusts in the Sonoran Desert (Organ Pipe Cactus National Monument, AZ). *FEMS Microbiology Ecology*, *54*(2), 233–245. https://doi.org/10.1016/j.femsec.2005.03.011

Nishiizumi, K., Imamura, M., Caffee, M. W., Southon, J. R., Finkel, R. C., & McAninch, J. (2007). Absolute calibration of 10Be AMS standards. *Nuclear Instruments and Methods in Physics Research Section B: Beam Interactions with Materials and Atoms*, *258*(2), 403–413. https://doi.org/10.1016/j.nimb.2007.01.297

Niu, Y., Gao, Z., Li, Y., & Luo, K. (2019). Effect of rock fragment content on erosion processes of disturbed soil accumulation under field scouring conditions. *Journal of Soils and Sediments*, *19*(4), 1708–1723. https://doi.org/10.1007/s11368-018-2200-3

Pearthree, P. A., & Scarborough, R. B. (1985). Reconnaissance analysis of possible Quaternary faulting in central Arizona. Arizona Geological Survey Open File Report, OFR-85-04, 1 map sheet, map scale. *1*(250), 75.

Placzek, C., Granger, D. E., Matmon, A., Quade, J., & Ryb, U. (2014). Geomorphic process rates in the central Atacama Desert, Chile: Insights from cosmogenic nuclides and implications for the onset of hyperaridity. *American Journal of Science*, *314*(10), 1462–1512. https://doi.org/10.2475/10.2014.03

Poesen, J., De Luna, E., Franca, A., Nachtergaele, J., & Govers, G. (1999). Concentrated flow erosion rates as affected by rock fragment cover and initial soil moisture content. *catena*, *36*(4), 315–329. https://doi.org/10.1016/S0341-8162(99)00044-2

Portenga, E. W., & Bierman, P. R. (2011). Understanding Earth's eroding surface with 10 Be. *GSA Today: A Publication of the Geological Society of America*, *21*(8), 4–10. https://doi.org/10.1130/G111A.1

Reiners, P. W., Carlson, R. W., Renne, P. R., Cooper, K. M., Granger, D. E., McLean, N. M., & Schoene, B. (2017). Cosmogenic nuclides. In P. W. Reiners, R. W. Carlson, P. R. Renne,

K. M. Cooper, D. E. Granger, N. M. McLean, & B. Schoene (Eds.), *Geochronology and Thermochronology* (pp. 395–420). Wiley Online Books. doi:10.1002/9781118455876

Reusser, L., Bierman, P., & Rood, D. (2015). Quantifying human impacts on rates of erosion and sediment transport at a landscape scale. *Geology*, *43*(2), 171–174. https://doi.org/10.1130/G36272.1

Richard, S. M., Reynolds, S. J., Spencer, J. E., & Pearthree, P. A. (2002). Digital graphics files for the geologic map of Arizona, a representation of Arizona Geological Survey map 35.

Riebe, C. S., Kirchner, J. W., Granger, D. E., & Finkel, R. C. (2001). Minimal climatic control on erosion rates in the Sierra Nevada, California. *Geology*, *29*(5), 447–450. https://doi.org/10.1130/0091-7613(2001)029<0447:MCCOER>2.0.CO;2

Ruetenik, G., Jansen, J. D., Val, P., & Ylä-Mella, L. (2022). Optimising global landscape evolution models with 10Be. *Earth Surface Dynamics Discuss*, 1–32. https://doi.org/10.5194/esurf-2022-54

Schaller, M., & Ehlers, T. A. (2022). Comparison of soil production, chemical weathering, and physical erosion rates along a climate and ecological gradient (Chile) to global observations. *Earth Surface Dynamics*, *10*(1), 131–150. https://doi.org/10.5194/esurf-10-131-2022

Schick, A. P., & Magid, D. (1978). Terraces in arid stream valleys a probability model. *Catena*, *5*(3–4), 237–250. https://doi.org/10.1016/0341-8162(78)90012-7

Seong, Y. B., Larson, P. H., Dorn, R. I., & Yu, B. Y. (2016). Evaluating process domains in small arid granitic watersheds: Case study of pima wash, South Mountains, Sonoran Desert, USA. *Geomorphology*, *255*, 108–124. https://doi.org/10.1016/j.geomorph.2015.12.014

Shafiqullah, M., Damon, P. E., Lynch, D. J., Reynolds, S. J., Rehrig, W. A., & Raymond, R. H. (1980). K-Ar geochronology and geologic history of southwestern Arizona and adjacent areas. *Studies in Western Arizona Arizona Geological Society Digest*, *12*, 201–260.

Shinker, J. J., & Bartlein, P. J. (2010). Spatial variations of effective moisture in the western United States. *Geophysical Research Letters*, *37*(2). https://doi.org/10.1029/2009GL041387

Skotnicki, S. J. (1996). Geologic map of the Bartlett dam quadrangle and southern part of the Horseshoe Dam quadrangle, Maricopa County, Arizona. *Arizona Geological Survey Open File Report*, *96-22*, 1–22.

Skotnicki, S. J., & DePonty, J. (2020). Subsurface evidence for the sudden integration of the Salt river across the internally drained basin and range Province, Arizona, USA. *Geomorphology*, *371*, 107429. https://doi.org/10.1016/j.geomorph.2020.107429

Skotnicki, S. J., & Leighty, R. S. (1997). Geological map of the Stewart Mountain Quadrangle, Maricopa County, Arizona. Arizona Geological Survey Open File Report OFR-97-12, 1 map sheet, map scale. *1*(24), 001–019.

Skotnicki, S. J., Seong, Y. B., Dorn, R. I., Larson, P. H., DePonty, J., & Jeong, A. (2021). Drainage integration of the Salt and Verde rivers in a basin and range extensional landscape, central Arizona, USA. *Geomorphology*, *374*, 107512. https://doi.org/10.1016/j.geomorph.2020.107512

Spencer, J. E., & Reynolds, S. J. (1989). Middle Tertiary tectonics of Arizona and adjacent areas. In J.P. Jenney, & S.J. Reynolds (Eds.), *Geologic evolution of Arizona: Arizona Geological Society Digest* (Vol. 17, pp. 539–574). Arizona Geological Society.

Spencer, J. E., & Reynolds, S. J. (1991). Tectonics of Mid-Tertiary Extension along a transect through west central Arizona. *Tectonics*, *10*(6), 1204–1221. https://doi.org/10.1029/91TC01160

Spencer, J. E., Richard, S. M., & Ferguson, C. A. (2001). Cenozoic structure and evolution of the boundary between the basin and range and transition Zone provinces in Arizona. In M. C. Erskine, J. E. Faulds, J. M. Bartley, & P. D. Rowley (Eds.), *The geologic transition, high plateaus to great basin - a symposium and field guide* (No. 30, pp. 273–289). Utah Geological Association.

Stamp, N. E., & Ohmart, R. D. (1978). Resource utilization by desert rodents in the lower Sonoran Desert. *Ecology*, *59*(4), 700–707. https://doi.org/10.2307/1938773

Übernickel, K., Pizarro-Araya, J., Bhagavathula, S., Paulino, L., & Ehlers, T. A. (2021). Reviews and syntheses: Composition and characteristics of burrowing animals along a climate and ecological gradient, Chile. *Biogeosciences*, *18*(20), 5573–5594. https://doi.org/10.5194/bg-18-5573-2021

U.S. Geological Survey, 2017, 1/3rd arc-second Digital elevation models (DEMs) - USGS National map 3DEP Downloadable data. Available at https://viewer.nationalmap.gov/basic/#/

Van Devender, T. R. (1990). Late Quaternary vegetation and climate of the Sonoran Desert, United States and Mexico. In J. L. Betancourt, T. R. Van Devender, & P. S. Martin (Eds.), *Packrat middens: the last 40,000 years of biotic change* (pp. 134–165). University of Arizona Press. https://doi.org/10.2307/j.ctv21wj578.10

Van Devender, T. R., Thompson, R. S., & Betancourt, J. L., 1987. Vegetation history of the deserts of southwestern North America: The nature and timing of the late Wisconsin-Holocene transition. North America and adjacent oceans during the last glaciation: The Geology of North America. Geological Society of America K3, pp.323–352

Van Leeuwen, W. J., Davison, J. E., Casady, G. M., & Marsh, S. E. (2010). Phenological character-ization of desert sky island vegetation communities with remotely sensed and climate time series data. *Remote Sensing*, 2(2), 388–415. https://doi.org/10.3390/rs2020388

von Bennewitz, E., & Aladro, J. (2017). The effects of rainfall intensity and rock fragment cover on soil hydrological responses in central chile. *Journal of Soil Science and Plant Nutrition*, 17(3), 781–793. https://doi.org/10.4067/S0718-95162017000300017

von Blanckenburg, F. (2005). The control mechanisms of erosion and weathering at basin scale from cosmogenic nuclides in river sediment. *Earth and Planetary Science Letters*, 237(3–4), 462–479. https://doi.org/10.1016/j.epsl.2005.06.030

Wackett, A. A., Yoo, K., Amundson, R., Heimsath, A. M., & Jelinski, N. A. (2018). Climate controls on coupled processes of chemical weathering, bioturbation, and sediment transport across hillslopes. *Earth Surface Processes and Landforms*, 43(8), 1575–1590. https://doi.org/10.1002/esp.4337

Weng, C., & Jackson, S. T. (1999). Late glacial and Holocene vegetation history and paleoclimate of the Kaibab Plateau, Arizona. *Palaeogeography, Palaeoclimatology, Palaeoecology*, 153(1–4), 179–201. https://doi.org/10.1016/S0031-0182(99)00070-X

Whitford, W. G., & Kay, F. R. (1999). Biopedturbation by mammals in deserts: A review. *Journal of Arid Environments*, 41(2), 203–230. https://doi.org/10.1006/jare.1998.0482

Willenbring, J. K., Codilean, A. T., & McElroy, B. (2013). Earth is (mostly) flat: Apportionment of the flux of continental sediment over millennial time scales. *Geology*, 41(3), 343–346. https://doi.org/10.1130/G33918.1

Xia, L., Song, X., Fu, N., Cui, S., Li, L., Li, H., & Li, Y. (2018). Effects of rock fragment cover on hydrological processes under rainfall simulation in a semi-arid region of China. *Hydrological Processes*, 32(6), 792–804. https://doi.org/10.1002/hyp.11455

Zhang, Y., Zhang, M., Niu, J., Li, H., Xiao, R., Zheng, H., & Bech, J. (2016). Rock fragments and soil hydrological processes: Significance and progress. *Catena*, 147, 153–166. https://doi.org/10.1016/j.catena.2016.07.012